

This article was downloaded by:

On: 25 January 2011

Access details: *Access Details: Free Access*

Publisher *Taylor & Francis*

Informa Ltd Registered in England and Wales Registered Number: 1072954 Registered office: Mortimer House, 37-41 Mortimer Street, London W1T 3JH, UK



Liquid Crystals

Publication details, including instructions for authors and subscription information:

<http://www.informaworld.com/smpp/title~content=t713926090>

Conformational effects on mesophase stability: numerical comparison of carborane diester homologous series with their bicyclo[2.2.2]octane, cyclohexane and benzene analogues

Piotr Kaszynski^a; Adam Januszko^a; Kiminori Ohta^b; Takashi Nagamine^b; Piotr Potaczek^a; Victor G. Young^c; Yasuyuki Endo^b

^a Organic Materials Research Group, Department of Chemistry, Vanderbilt University, Nashville, TN 37235 ^b Tohoku Pharmaceutical University, Aoba-ku, Sendai 981-8558, Japan ^c X-ray Crystallographic Laboratory, Department of Chemistry, University of Minnesota, Twin Cities, MN 55455

To cite this Article Kaszynski, Piotr , Januszko, Adam , Ohta, Kiminori , Nagamine, Takashi , Potaczek, Piotr , Young, Victor G. and Endo, Yasuyuki(2008) 'Conformational effects on mesophase stability: numerical comparison of carborane diester homologous series with their bicyclo[2.2.2]octane, cyclohexane and benzene analogues', *Liquid Crystals*, 35: 10, 1169 – 1190

To link to this Article: DOI: 10.1080/02678290802409775

URL: <http://dx.doi.org/10.1080/02678290802409775>

PLEASE SCROLL DOWN FOR ARTICLE

Full terms and conditions of use: <http://www.informaworld.com/terms-and-conditions-of-access.pdf>

This article may be used for research, teaching and private study purposes. Any substantial or systematic reproduction, re-distribution, re-selling, loan or sub-licensing, systematic supply or distribution in any form to anyone is expressly forbidden.

The publisher does not give any warranty express or implied or make any representation that the contents will be complete or accurate or up to date. The accuracy of any instructions, formulae and drug doses should be independently verified with primary sources. The publisher shall not be liable for any loss, actions, claims, proceedings, demand or costs or damages whatsoever or howsoever caused arising directly or indirectly in connection with or arising out of the use of this material.

Conformational effects on mesophase stability: numerical comparison of carborane diester homologous series with their bicyclo[2.2.2]octane, cyclohexane and benzene analogues

Piotr Kaszynski^{a*}, Adam Januszko^a, Kiminori Ohta^b, Takashi Nagamine^b, Piotr Potaczek^{a**}, Victor G. Young Jr.^c and Yasuyuki Endo^b

^aOrganic Materials Research Group, Department of Chemistry, Vanderbilt University, Nashville, TN 37235, USA; ^bTohoku Pharmaceutical University, 4-4-1, Komatsushima, Aoba-ku, Sendai 981-8558, Japan; ^cX-ray Crystallographic Laboratory, Department of Chemistry, University of Minnesota, Twin Cities, MN 55455, USA

(Received 24 July 2008; accepted 14 August 2008)

Three series of diesters of 4-alkoxyphenols containing 12-vertex *p*-carborane (**1A**[*n*], *n*=1–22), 10-vertex *p*-carborane (**1B**[*n*], *n*=1–12) or bicyclo[2.2.2]octane (**1C**[*n*], *n*=1–12) as the central structural element were prepared and investigated by optical and calorimetric methods. All carborane diesters exhibited exclusively nematic behaviour, whereas the carbocyclic analogues **1C**[*n*] and also cyclohexane (**1D**[*n*]) and benzene (**1E**[*n*]) derivatives, showed early onset of SmA phase and complete disappearance of nematic behaviour. The isotropic transition temperatures, T_{MI} , for the five series of mesogens were analysed numerically using a three-parameter exponential function. The resulting limiting values, $T_{MI}(\infty)$, provided a quantitative assessment of the central element ability to support the mesogenic state. They demonstrated that, whereas the $T_{MI}(\infty)$ values for the carbocycles, **C**, **D**, and **E**, are around 125°C, for carboranes **A** and **B** this value is $70 \pm 2^\circ\text{C}$ and $49 \pm 19^\circ\text{C}$, respectively. Two types of comparative analysis of trends in T_{MI} relative to those of the terephthalate series **1E**[*n*] demonstrated abnormal behaviour of both carborane series (**1A**[*n*] and **1B**[*n*]) and also the cyclohexane series (**1D**[*n*]). The former showed progressive destabilisation of the mesophase, whereas the series **1D**[*n*] exhibited increasing mesophase stability relative to **1E**[*n*] with increasing chain length. Both of these effects were explained using conformational analysis of theoretical models and experimental molecular structures for **1A**[3], **1B**[4] and **1C**[4]. The increasing relative destabilisation of the mesophase in the carborane derivatives was rationalised by the high order rotational axes in **A** and **B** and D_{4d} symmetry for **B**. The trend of the ΔT_{MI} values for series **1D**[*n*] was explained with the existence of the equatorial-axial conformational equilibrium for the cyclohexane derivatives. The clearing temperatures for the hypothetical pure diequatorial conformers **1D**[*n*]-**ee** were estimated.

Keywords: carborane; homologous series; nematic; conformation; numerical analysis

1. Introduction

Accumulated empirical data (1) demonstrates that the stability of liquid crystal phases is related to molecular conformational effects (2). In general, the increase in molecular flexibility leads to a decrease of phase stability presumably due to the lower dynamic aspect ratio and lower packing density in the liquid crystalline phase. This is readily apparent from the trends in homologous series, in which the increase of the chain length results in the decreases of the clearing temperature for high temperature materials. There are fewer studies of conformational effects in the rigid core and their impact on the mesophase stability. The best example is the equatorial-axial conformational equilibrium in cyclohexane (2) and other cyclic derivatives (3, 4) that affect the dynamic molecular shape and consequently the phase stability. Another type of conformational mobility is related to the symmetry of the core element and the number of available rotational conformational minima. Its

significance for mesophase stability began to emerge through our work with liquid crystalline derivatives of *p*-carboranes **A** and **B** (Figure 1), which possess 5-fold and 4-fold rotational axes, respectively (5–8). We have found that carboranes **A** and **B** exhibit generally lower effectiveness in stabilisation of mesophases as compared with bicyclo[2.2.2]octane (**C**), cyclohexane (**D**) and benzene (**E**) structural analogues that have lower order of rotational axes (9–13). A dramatic demonstration of the importance of the restricted rotation on phase stability is provided by the replacement of the $-\text{CH}_2\text{CH}_2-$ with $-\text{C}\equiv\text{C}-$ in carborane mesogens, which lowered the T_{NI} by over 150 K (5). Our results also demonstrated a possible link between the rotational axes order and the helical twisting power for chiral dopants (12).

Recently, we began to study short homologous series of carborane-containing mesogens and their comparison with the available mesogenic carbocyclic analogues (10, 11). In all carborane derivatives, the

*Corresponding author. Email: piotr.kaszynski@vanderbilt.edu

**A visiting student from the laboratory of Prof. Jacek Młochowski of Wrocław Polytechnic, Wrocław, Poland.

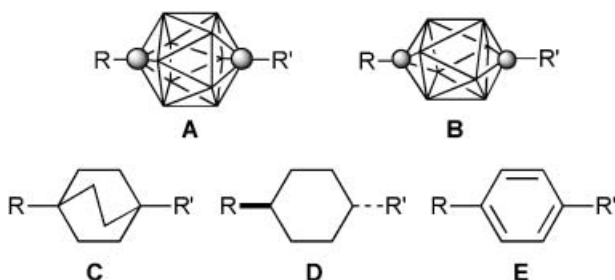
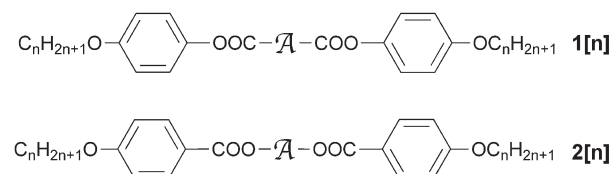


Figure 1. 1,12-Dicarba-*closo*-dodecaborane (12-vertex *p*-carborane, **A**), 1,10-dicarba-*closo*-decaborane (10-vertex *p*-carborane, **B**), bicyclo[2.2.2]octane (**C**), cyclohexane (**D**) and benzene (**E**). In **A** and **B** each vertex corresponds to a BH fragment and the sphere represents a carbon atom.

nematic phase prevails and even the longest homologues exhibit pure nematic behaviour, whereas in the carbocyclic analogues the onset of smectic phases is observed much earlier in the series. These and other results (5–7, 9–13) indicate that carboranes typically inhibit smectogenic properties relative to their carbocyclic structural analogues. We became interested in the limits of the nematic behaviour in the carborane derivatives and also in numerical assessment of the ring effectiveness in supporting the low order mesophases [nematic and smectic A (SmA) phases]. Therefore, we focused on a series of diesters **1[n]**, which is readily accessible and for which many carbocyclic analogues have been well studied.

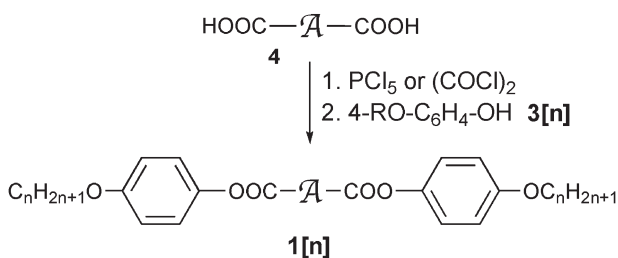
In this paper, we report the synthesis and characterisation of two homologous series of carborane derivatives **1A[n]** ($n \leq 22$) and **1B[n]** ($n \leq 12$). For comparison purpose, we also prepared the isostructural series of bicyclo[2.2.2]octane derivatives **1C[n]** ($n \leq 12$) and all three series were compared with the previously reported cyclohexane (14, 15) **1D[n]** ($n \leq 16$), and benzene (15–18) **1E[n]** ($n \leq 12$) analogues. The nematic–isotropic (N–I) transition temperatures were numerically analysed with an exponential function to obtain parameters for the central ring. The results are discussed in the context of alkyl chain length and conformational properties of the central ring. The conformational analysis is aided by single crystal molecular structure for two carborane and one bicyclo[2.2.2]octane derivatives. We also briefly discuss the effect of the –COO– group orientation (**1[n]** and **2[n]**) on mesogenic properties in selected compounds.



2. Results

Synthesis

Diesters **1A[n]**–**1C[n]** were prepared from appropriate carboxylic acid chlorides and phenols **3[n]** in the presence of a base (**1A[n]** and **1B[n]**) or by refluxing in CCl₄ (**1C[n]**), as shown in Scheme 1. The latter method of esterification by alcoholysis of acid chlorides avoids the decarbonylation observed in the former method for bicyclo[2.2.2]octane-1,4-dicarbonyl chloride.

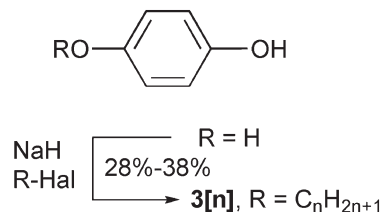


Scheme 1. Preparation of diesters **1A[n]**–**1C[n]**.

The required acid chlorides were prepared from the corresponding 1,12-dicarba-*closo*-dodecaborane-1,12-dicarboxylic acid (19) (**4A**) and 1,10-dicarba-*closo*-decaborane-1,10-dicarboxylic acid (**4B**) (20), and a stoichiometric amount of PCl₅ in benzene. Alternatively, the former acid chloride was prepared using oxalyl chloride. Bicyclo[2.2.2]octane-1,4-dicarboxylic acid (**4C**) (21), obtained by basic hydrolysis of the corresponding diethyl ester (22, 23), was converted into 1,4-bis(chlorocarbonyl)bicyclo[2.2.2]octane using PCl₅ and a small amount of POCl₃ as a solvent. All acid chlorides were used without further purification.

The pentyloxy derivative **2C[5]** was prepared by esterification of bicyclo[2.2.2]octane-1,4-diol (23) with 4-pentyloxybenzoyl chloride.

4-Nonyloxyphenol (**3[9]**) was prepared according to an analogous literature method (24) involving statistical alkylation of hydroquinone in aqueous EtOH. Higher 4-alkoxyphenols **3[n]** were obtained in DMF in the presence of NaH (25) (Scheme 2).






Scheme 2. Preparation of 4-alkoxyphenols **3[n]**.

Mesogenic properties

Transition temperatures and enthalpies for series **1A[n]**, **1B[n]** and **1C[n]** were determined by differential

Table 1. Transition temperatures (°C) and enthalpies (kJ mol⁻¹) for **1[n]** (Cr=crystal, Sm=smectic, N=nematic, I=isotropic).

$$C_nH_{2n+1}O-\text{C}_6\text{H}_4-\text{OOC}-\mathcal{A}-\text{COO}-\text{C}_6\text{H}_4-\text{OC}_nH_{2n+1} \quad \mathbf{1[n]}$$

\mathcal{A}	A	B	C
n			
1	Cr 219 N 239.4 I (43.8) (2.0)	Cr 148 N 230.2 I (38.6) (2.3)	Cr 155 N 272.7 I (28.4) (0.6)
2	Cr 216 N 238.0 I (48.5) (2.4)	Cr 204 N 234.8 I (49.1) (2.3)	Cr 134 N 273.4 I (39.8) (2.2)
3	Cr 198 (N 195.0) I (53.5) (1.9)	Cr 188 N 195.1 I (50.3) (1.8)	Cr ₁ 128 Cr ₂ 137 N 236.7 I (13.6) (37.3) (1.6)
4	Cr 137 N 182.6 I (37.1) (2.1)	Cr 70 Cr 111 N 183.4 I (6.8) (32.2) (2.7)	Cr 112 N 229.5 I (35.0) (0.9)
5	Cr 115 N 157.5 I (50.4) (1.3)	Cr 98 N 154.5 I (49.5) (1.8)	Cr ₁ 79 Cr ₂ 101 SmA 157 N 208.0 I (21.4) (17.3) (0.3) (1.3)
6	Cr 116 N 148.9 I (53.7) (1.9)	Cr 65 Cr 80 N 145.6 I (13.0) (25.9) (1.8)	Cr ₁ 77 Cr ₂ 103 SmA 176 N 200.4 I (13.8) (18.0) (0.8) (1.0)
7	Cr 108 N 134.0 I (52.6) (1.4)	Cr 86 N 129.5 I (60.2) (2.0)	Cr ₁ 86 Cr ₂ 94 SmA 182 N 188.6 I (20.0) (19.1) (1.6) (1.2)
8	Cr 95 N 128.4 I (47.6) (1.9)	Cr 64 N 124.9 I (45.4) (1.9)	Cr 94 (SmB 82.5 SmC 90) SmA 181.4 N 183.0 I (40.5) (0.4) (0) (1.8) (0.7)
9	Cr 85 N 119.5 I (64.3) (1.5)	Cr 75 N 115.8 I (64.0) (1.3)	Cr 96 (SmC 93) SmA 178.8 I (44.2) (0.6) (7.1)
10	Cr 66 N 116.1 I (44.4) (1.9)	Cr 66 N 112.4 I (46.4) (1.4)	Cr 96 SmC 100.0 SmA 175.1 I (44.5) (1.2) (8.2)
12	Cr 64 N 107.7 I (63.0) (1.8)	Cr ^c 68 N 104.3 I (35.8) (1.6)	Cr 93 SmC 104.9 SmA 166.9 I (49.2) (2.3) (9.8)
14	Cr 68 N 99.8 I (86.6) (1.8)	–	–
16	Cr 76 N 96.0 I (105.0) (1.9)	–	–
18	Cr 82 N 91.6 I (117.7) (2.3)	–	–
20	Cr 85 N 87.8 I (135.3) (2.3)	–	–
22	Cr 91 (N 85.5) I (155.6) (2.3)	–	–

^aLit.(31) Cr 152 N 269 I. ^bLit.(28) Cr 114 N 230 I. ^cCr–Cr transition at 65°C (7.8 kJ mol⁻¹).

scanning calorimetry (DSC) and results are shown in Table 1. Phase structures were assigned by comparison of microscopic textures observed in polarised light with those published for reference compounds and established trends in thermodynamic stability (26).

In general, carborane derivatives exhibit enantiotropic nematic phases, which crystallise upon cooling. The only exceptions are **1A[3]** and **1A[22]**, which form monotropic nematic phases 3 K and 5 K, respectively, below melting. Clearing temperatures, T_{NI} , for both carborane series **1A[n]** and **1B[n]** are similar, and they decrease with increasing length of the alkyl chain in the homologous series, as shown in Figure 2. In contrast, melting points of the 10-vertex *p*-carborane diesters in series **1B[n]** are generally lower than those

for the 12-vertex analogs **1A[n]**. The difference is about 20 K except for the methoxy derivatives **1A[1]** and **1B[1]** for which the difference is 71 K. The lower melting points for the 10-vertex derivatives results in a generally wider nematic phase range for **1B[n]** as compared to **1A[n]**.

Bicyclo[2.2.2]octane-1,4-dicarboxylates **1C[n]** form enantiotropic nematic phases. Smectic behaviour appears in the series beginning with the pentyloxy derivative **1C[5]**, and completely replaces the nematic phase in **1C[9]** (Figure 2(c)). The predominant SmA phase in the series is supplemented by a SmC phase starting at **1C[9]** and a monotropic smectic B (SmB) phase that appears in **1C[8]**. The early onset of smectic properties in **1C[n]** is similar

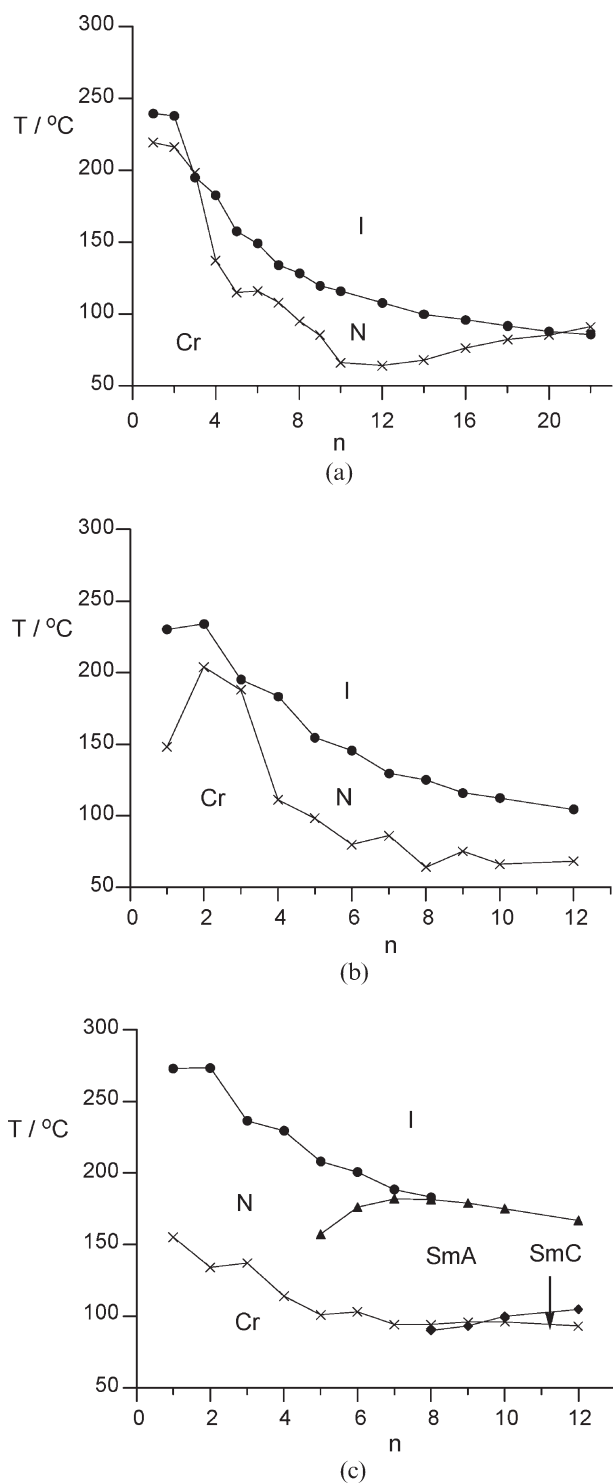


Figure 2. Transition temperatures versus the terminal chain length for (a) **1A**[*n*], (b) **1B**[*n*] and (c) **1C**[*n*]. The monotropic SmB phase for **1C**[8] is not shown. The lines are guides for the eye.

to that reported for cyclohexane series **1D**[*n*] (onset for **1D**[4]) and terephthalates **1E**[*n*] (onset for **1E**[5]). In the latter two series, the complete disappearance

of the nematic phase in favor of pure smectic behavior is observed for **1D**[7] and **1E**[12] (27). Our results for **1C**[4] confirmed an earlier finding (28), but significantly disagree with another report (29). Also, the transition temperatures for **1C**[1] were found to be about 3 K higher than those reported earlier (30, 31).

The entropy of the N-I transition is generally higher for the carborane derivatives (mean value for **1A**[*n*] is $4.1 \pm 0.6 \text{ J mol}^{-1} \text{ K}^{-1}$ and for **1B**[*n*] is $4.6 \pm 0.6 \text{ J mol}^{-1} \text{ K}^{-1}$) than for bicyclo[2.2.2]octane diesters **1C**[*n*] ($2.4 \pm 0.9 \text{ J mol}^{-1} \text{ K}^{-1}$). The latter is comparable with the average entropy of clearing obtained for the cyclohexane ($1.9 \pm 0.6 \text{ J mol}^{-1} \text{ K}^{-1}$) and terephthalate ($2.6 \pm 0.6 \text{ J mol}^{-1} \text{ K}^{-1}$) homologous series **1D**[*n*] and **1E**[*n*]. The latter entropy change values were calculated from the reported transition enthalpies and temperatures for **1E**[1] (15), **1E**[2] (15), **1E**[4] (15), **1E**[5]–**1E**[7] (18), **1E**[8] (32).

Comparative studies

Mesogenic properties of the three series of diesters in Table 1 were compared with the available literature data for series of cyclohexane-1,4-dicarboxylates (14, 33) **1D**[*n*] and terephthalates **1E**[*n*]. The former series has been investigated up to the octadecyloxy derivative **1D**[18], and reliable transition temperatures and enthalpies have been reported (14, 33). Transition temperatures for terephthalates **1E**[*n*] first obtained for *n*=1–6 by microscopic determination (16) were consistent with later calorimetric results (18) for **1E**[5] and **1E**[6], and were used here for the comparison. Other reports provided transition temperatures for higher homologues **1E**[7] (18), **1E**[8] (32), **1E**[10] (34), and **1E**[12] (27).

Clearing temperatures in **1**[*n*].

An assessment of the effectiveness of the central rings A–E on the mesophase stability was performed by numerical analysis of trends in clearing temperatures (N-I, SmA-I, and SmC-I) for each individual series and also relative to the effectiveness of the benzene ring (E) in the terephthalate series **1E**[*n*].

The clearing temperatures for odd and even members of each of the five homologous series of diesters **1A**–**1E** can be described by the exponential function

$$T_{MI}(n) = T_{MI}(\infty) + \exp(an^c + b). \quad (1)$$

The function for odd and function for the even members of the series asymptotically approach the common limit with the increasing chain length of the alkyl chain. The value of this limit is indicative of

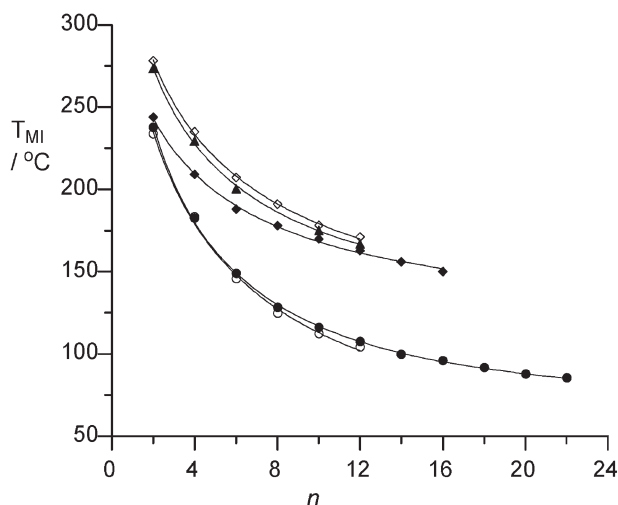


Figure 3. N-I or SmA-I transition temperatures for diesters **1**[*n*] and the best fit lines: **1A**[*n*] (full circles) $T_{MI}=70+\exp(6.16 - 0.73\sqrt{n})$; **1B**[*n*] (open circles), $T_{MI}=49+\exp(6.09 - 0.61\sqrt{n})$; **1C**[*n*] (triangles), $T_{MI}=129+\exp(5.9 - 0.65\sqrt{n})$; **1D**[*n*] (diamonds), $T_{MI}=126+\exp(5.5 - 0.58\sqrt{n})$; **1E**[*n*] (open diamonds), $T_{MI}=123+\exp(5.87 - 0.58\sqrt{n})$. $R^2 \geq 0.997$.

the ability of the rigid core to support the mesophase. For the numerical analysis we selected compounds with even number of carbon atoms in the chain and the results are shown in Figure 3.

Initial attempts at fitting the T_{MI} values for **1A**[*n*] to the four-parameter function in Equation (1) demonstrated, not surprisingly, that all constants depend on the number of datapoints (Table 2). Closer inspection revealed that the value of the factor c in Equation (1) exhibits an exponential dependence on n . Therefore, its value at infinity, $c(\infty)$, could be extrapolated from $c(n)$ values using the same four-parameter function, Equation (1), in which $c=1$.

Fitting only five data points for T_{MI} values ($n \leq 10$) gives unreliable results. Also fitting the first seven points ($n \leq 14$) gave the $c(14)$ value with a large error and clearly lying outside the correlation, presumably due to the T_{NI} for **1A**[14] measured

lower by 1 K. Therefore, values of parameter $c(n)$ that were obtained from fitting 6 data points [$c(12)$, $n \leq 12$] and also 8 [$c(16)$, $n \leq 16$], 9 [$c(18)$, $n \leq 18$], 10 [$c(20)$, $n \leq 20$] and 11 data points [$c(22)$, $n \leq 22$] were used, and the extrapolated value of the exponent $c(\infty)$ for infinite number of data points ($n=\infty$) is 0.51 ± 0.04 and $T_{NI}(\infty)=69 \pm 3$ (Table 2). Consequently, the exponent c in Equation (1) was set at 0.5 and all series of T_{MI} values for diesters **1A**[*n*]-**1E**[*n*] were fitted to the three-parameter function, Equation (2).

$$T_{MI} = T_{MI}(\infty) + \exp(a\sqrt{n} + b). \quad (2)$$

Numerical results in Figure 3 show that the carbocyclic derivatives **1C**[*n*], **1D**[*n*] and **1E**[*n*] approach practically the same limit $\left[\lim_{n \rightarrow \infty} T_{MI}(n) = T_{MI}(\infty) \right]$ of about 125°C (Table 3). In contrast, the limiting values for both carborane derivatives are much lower and are 70°C and 26°C for **1A**[*n*] and **1B**[*n*], respectively. The extrapolated value for the former is practically identical with that obtained for the extrapolation from the partial data set in Table 2 (*vide supra*). The error associated with each $T_{MI}(\infty)$ value reflects the number of data points used for fitting and the quality and consistency of the data within each series. Thus, the uncertainty for the two shortest series, **1B**[*n*] and **1C**[*n*], is high, whereas for the longest series, **1A**[*n*], is less than 2 K. The particularly large error for the limiting value for **1B**[*n*] series may also be related to the difficulties with fine purification of **1B**[10] by recrystallisation.

Overall, the results indicate that the effectiveness of the central ring in **1** in stabilisation of mesophase follows $C \sim D \sim E > A > B$.



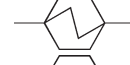
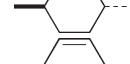
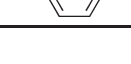
Since even members and odd members of a homologous series have the same limit for $n=\infty$, then the $T_{MI}(\infty)$ values obtained from fitting the one part of the series can be used for fitting the other part of the series with fewer data points. This treatment provides a predictive tool for assessing the clearing points of higher members of the homologous series. Thus, the $T_{MI}(\infty)$ values obtained for even members

Table 2. Constants for the four-parameter fitting function, i.e. Equation (1), approximating T_{NI} of **1A**[*n*] (for all fittings $R^2 > 0.999$; errors are shown in parentheses).

Data points	$n \leq$	$T_{NI}(\infty)$	a	b	c
5	10	97.5(4)	-0.244	5.437	1.014(8)
6	12	94.4(15)	-0.267	5.486	0.96(4)*
7	14	85.9(50)	-0.347	5.635	0.81(10)
8	16	84.9(31)	-0.359	5.654	0.79(7)*
9	18	82.2(27)	-0.396	5.71	0.74(7)*
10	20	79.0(29)	-0.447	5.79	0.69(7)*
11	22	77.3(25)	-0.477	5.83	0.66(6)*
extrapol. ^a	∞	69 ± 3	-	-	0.51(4)

^aObtained from fitting values denoted with the asterisk to Equation (1) in which $c=1$.

Table 3. The limiting values for clearing temperatures $T_{MI}(\infty)$ obtained for even members of each diester series **1[n]** using Equation (2).

Series	\mathcal{A}	Data points	$T_{MI}(\infty)$
1A[n]		11	70 ± 12
1B[n]		6	49 ± 19
1C[n]		6	129 ± 10
1D[n]		8	126 ± 6
1E[n]		6	123 ± 8

of each series **1A[n]**–**1E[n]**, were substituted into Equation (2) and used for fitting the odd members of each series. The datapoints for $n=1$ were not used since they were clearly outside the correlation. The remaining four (**1A[n]**–**1C[n]**) or three (**1E[n]**) data points were fitted giving the following best fit lines: **1A[n]** $T_{MI}=70+\exp(6.09-0.73\sqrt{n})$; **1B[n]** $T_{MI}=49+\exp(6.08-0.63\sqrt{n})$; **1C[n]**, $T_{NI}=129+\exp(5.76-0.62\sqrt{n})$; **1E[n]**, $T_{NI}=123+\exp(5.68-0.53\sqrt{n})$; $R^2 \geq 0.999$. For the cyclohexane series **1D[n]** there were only two data points besides **1D[1]**, which were insufficient for obtaining a meaningful fitting.

Another way to assess the impact of the central ring on the mesophase stability is accomplished by comparative studies using diester series **1E[n]** as the reference. Thus, Figure 4 shows the difference between T_{MI} values for each series and $T_{MI}(\mathbf{E})$ for the terephthalates **1E[n]** plotted as a function of the alkyl chain length n , whereas Figure 5 presents a linear correlation of T_{NI} values for **1A[n]**–**1D[n]** with those of **1E[n]** in the range of $n=1$ – 12 .

Analysis of the plot in Figure 4 shows that the clearing temperatures for the bicyclo[2.2.2]octane series **1C[n]** are generally lower than those of the terephthalates **1E[n]** by approximately a constant value of 6 K ($\Delta T_{MI} = -5.5 \pm 1.8$ K). This is reflected in a slope k of the line correlating the T_{MI} values for **1C[n]** and **1E[n]** that is practically a unity ($k=0.99 \pm 0.02$, Figure 5). In contrast, the relative values T_{MI} in series **1A[n]**, **1B[n]** and **1D[n]** systematically vary with increasing n . The plots for **1A[n]** and **1B[n]** exhibit descending behaviour, which indicates increasing destabilisation of the nematic phase in the carborane derivatives relative to terephthalates **1E[n]** with increasing alkyl chain

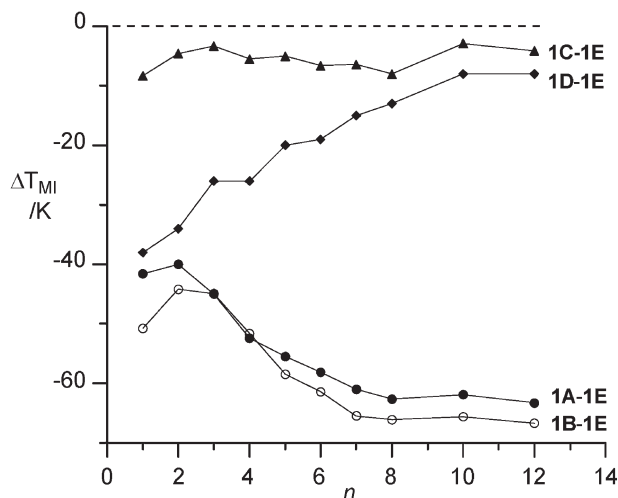


Figure 4. The T_{MI} for diesters **1A[n]** (full circles), **1B[n]** (open circles), **1C[n]** (triangles) and **1D[n]** (diamonds) relative to that of the terephthalates **1E[n]** ($\Delta T_{MI}=T_{MI}-T_{MI}(\mathbf{E})$). The lines are guides for the eye.

length. The curve for cyclohexane diesters **1D[n]** shows opposite behaviour and indicates that the mesophase in **1D[n]** becomes more stable relative to terephthalates **1E[n]** for higher homologues. This behaviour is well-reflected in T_{MI} correlations shown in Figure 5. The slopes k for the two carborane series are significantly larger than unity ($k=1.24 \pm 0.02$ for

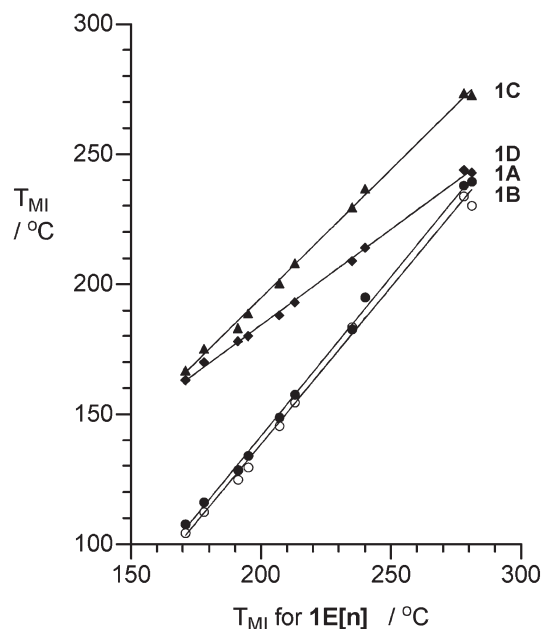


Figure 5. A plot of the T_{MI} for diesters **1A[n]** (full circles), **1B[n]** (open circles), **1C[n]** (triangles) and **1D[n]** (diamonds) against T_{MI} of the terephthalates **1E[n]**. Best fit lines: **1A[n]**: $T_{NI}(\mathbf{A})=-103.4+1.225T_{NI}(\mathbf{E})$; **1B[n]**: $T_{NI}(\mathbf{B})=103.1+1.208T_{NI}(\mathbf{E})$; **1C[n]**: $T_{NI}(\mathbf{C})=-3.1+0.989T_{NI}(\mathbf{E})$; **1D[n]**: $T_{NI}(\mathbf{D})=36.8+0.737 \times T_{NI}(\mathbf{E})$. $R^2 \geq 0.993$.

1A[n] and $k=1.22 \pm 0.05$ for **1B[n]**), whereas the slope for the cyclohexane diesters **1D[n]** is significantly smaller than unity ($k=0.76 \pm 0.02$).

The results shown in Figures 4 and 5 are consistent with those in Figure 3 and demonstrate that the bicyclo[2.2.2]octane and terephthalate series behave similarly, whereas the carborane derivatives and cyclohexane diesters exhibit a relatively abnormal behaviour in the homologous series.

The orientation of the COO group.

The availability of the **1C[n]** series allows for an analysis of the effect of the ester group orientation on the mesophase stability by comparison with the data reported for bicyclo[2.2.2]octane-1,4-diol dibenzoates **2C[n]** (23) and also **2C[5]**. This complements the two other series of pairs of isomeric mesogens: **1D[n]** and cyclohexane-1,4-diol diesters **2D[n]** (23, 35), and also terephthalates **1E[n]** and hydroquinone diesters **2E[n]** (23, 35). A plot of T_{MI} for dibenzoates **2[n]** relative to T_{MI} for the isomeric diesters **1[n]** shows little change in mesophase stability for bicyclo[2.2.2]octane and benzene pairs of mesogens (Figure 6). The former exhibits a small decrease (mean $\Delta T_{MI} = -6 \pm 5$ K) and the latter a small enhancement (mean $\Delta T_{MI} = 6 \pm 2.3$ K, excluding $n=1$) in stability of the nematic phase in the dibenzoate series **2[n]** relative to series **1[n]**. In contrast, the orientation of the COO group in the cyclohexane isomeric pairs has a significant impact on mesophase stability, and the dibenzoate series **2D[n]** has generally lower T_{MI} than the **1D[n]** isomers by an average of 48 ± 4 K. Plots for all three series of isomers show slow descending character for the lower members of each series and apparent stabilisation of ΔT_{MI} for higher homologues at about -11 K for **C** and $+4$ K for **E**.

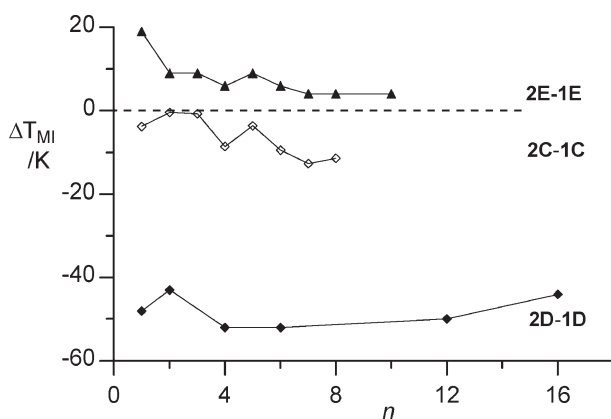


Figure 6. The difference in T_{MI} for pairs of isomeric diesters **1C[n]** and **2C[n]** (triangles), **1D[n]** and **2D[n]** (diamonds), and **1E[n]** and **2E[n]** (open diamonds). $\Delta T_{MI} = T_{MI}(2) - T_{MI}(1)$. The lines are guides for the eye.

Numerical analysis for even members of series **2C[n]** and **2E[n]** using Equation (2) shows that the limiting values $T_{MI}(\infty)$ are lower than those for the isomers **1C[n]** and **1E[n]** and are $87 \pm 7^\circ\text{C}$ and $113 \pm 5^\circ\text{C}$, respectively.

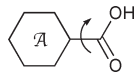
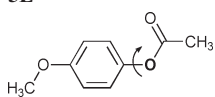
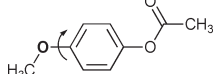
Conformational analysis

For a better understanding of both static and dynamic shapes of the molecules in each series, we performed quantitative conformational analysis of monocarboxylic acids **5** using the DFT and MP2 methods (36, 37) (Table 4 and Figure 7), which gave the bases for qualitative conformation analysis of diacids **4** shown in Figure 8. Table 4 also contains rotational transitional state energies for two other structural elements of the diesters: the Ph-OAc and Ph-OMe bonds.

Results in Table 4 show that the carboxyl group adopts an eclipsed (**5A**, **5E**), nearly eclipsed (**5C** and **5D**) or staggered (**5B**) conformation in the ground state geometry. In the transition state, the carboxyl group is staggered in benzoic acid (**5E**), pseudo-staggered in **5C**, or eclipsed in carborane derivatives **5A** and **5B**. The highest barrier to internal rotation around the A-COOH bond is calculated for **5E** ($\Delta E^\ddagger = 5.8 \text{ kcal mol}^{-1}$), which results from strong electronic interactions between the COOH group and the ring. The remaining compounds have significantly lower barriers to internal rotation and much weaker or non-existent electronic coupling between the two molecular fragments (39). For alicyclic carboxylic acids **5C** and **5D** the activation energy ΔE^\ddagger is over four times lower than that for benzoic acid **5E**, and these values are comparable to those calculated for 4-MeO-C₆H₄-OAc (Table 4). The activation energies are lowest for the carborane derivatives **5A** and **5B**, and the ΔG^\ddagger for the former is solely due to the entropy change in the TS.

The symmetry of the parent ring A determines the number of minima on the potential energy surface (PES). Thus, the number of minima in acids **5** increases from 2 for **5E** to 5 in **5A**. The cyclohexane derivative **5D** has a complicated PES with three conformational minima (Figure 7). Two rotamers are separated by a low barrier ΔE^\ddagger of $0.3 \text{ kcal mol}^{-1}$ and constitute an enantiomeric pair. The third minimum has C_s point group symmetry, has higher energy by $0.6 \text{ kcal mol}^{-1}$ and is accessible through a barrier $\Delta E^\ddagger = 1.2 \text{ kcal mol}^{-1}$. The orientation of the COOH group relative to the cyclohexane ring in the global minimum with the C-C-C=O dihedral angle of $\theta = 17^\circ$ (Table 4) is consistent with the solid-state structure for a 4-substituted cyclohexanecarboxylic acid ($\theta = 20.2^\circ$) (40) and its ester ($\theta = 16.8^\circ$) (41), cyclohexane-1,4-dicarboxylic acid ($\theta = 7.4^\circ$) (42) and

Table 4. Calculated barriers to internal rotation and conformational properties of monocarboxylic acids **5** (MP2/6-31G(d) level with B3LYP/6-31G(d) thermodynamic corrections).

	ΔE^\ddagger ^a	ΔG^\ddagger_{298}	θ ^b		Symmetry	
			GS	TS	GS	TS
5A	0.0	1.2	35	0	C_s	C_s
5B	0.75	2.0	45	0	C_s	C_s
5C ^c	1.2	2.6	3.7 ^d	47	C_1	C_1
5D ^e	1.2	2.5	17	56	C_1	C_1
5E	5.8	6.75	0	90	C_s	C_s
	1.3	2.6	116	0	C_1	C_s
	1.7	2.2	0.9	64	C_1	C_1

^aCalculated as Δ SCF and ZPE. ^bThe X–C–C=O for acids and X–C–O–C for phenyl acetate dihedral angle. X=B for **A** and **B** and X=C for **C–E**. ^cRing twist angle 17°. ^dAngle θ varies from 7.7° to 23.6° in the experimental structure of a 4-pentylbicyclo[2.2.2]octane-1-carboxylate ester (**38**). ^eLocal minimum at $\theta=0^\circ$: $\Delta E=0.6$ kcal mol⁻¹, $\Delta G=0.5$ kcal mol⁻¹; rotational transition state between two enantiomeric global minima at $\theta=60.7^\circ$: $\Delta E^\ddagger=0.3$ kcal mol⁻¹, $\Delta G^\ddagger_{298}=1.5$ kcal mol⁻¹. See Figure 7.

its mesogenic derivatives (**43**). The shape of the PES for **5D** (Figure 7) and the existence of two minima are in qualitative agreement with computational results for cyclohexanecarbaldehyde and two acyl halides derived from **5D** (**44**).

The conformational analysis for monocarboxylic acids **5** indicates that two carboxyl groups in diacids **4** can adopt 2–5 relative orientations depending on the symmetry of the parent ring (Figure 8). Closer qualitative analysis demonstrates that, with the exception of the 10-vertex carborane derivative **4B**,

carboxyl groups in all diacids can adopt coplanar orientation in their rotational ground states. Out of those, only in diacids **4A**, **4D** and **4E** the two carboxyl groups can form antiperiplanar rotamers that are most favourable for supporting a mesophase. In benzoic acids both rotamers are planar (antiperiplanar and synperiplanar). In contrast, there are two gauche rotamers in the bicyclo[2.2.2]octane derivative **4C** (an enantiomeric pair) and four in 12-vertex carborane diacid **4A** (two enantiomeric pairs) in addition to the coplanar ones. In the cyclohexane

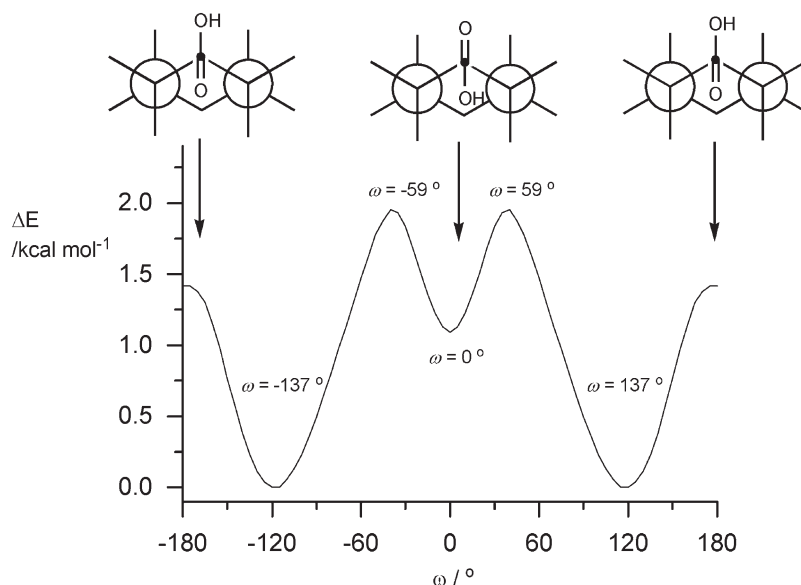


Figure 7. Potential energy surface for rotation around the C–COOH bond in cyclohexanecarboxylic acid **5D** obtained using the B3LYP/3-21G(d) method. ΔE is the difference in the total SCF energy. The angle ω is defined as $H_{ax}-C(1)-C=O$. The values of ω for conformational extrema are reported for the MP2/6-31G(d) geometry optimisation results.

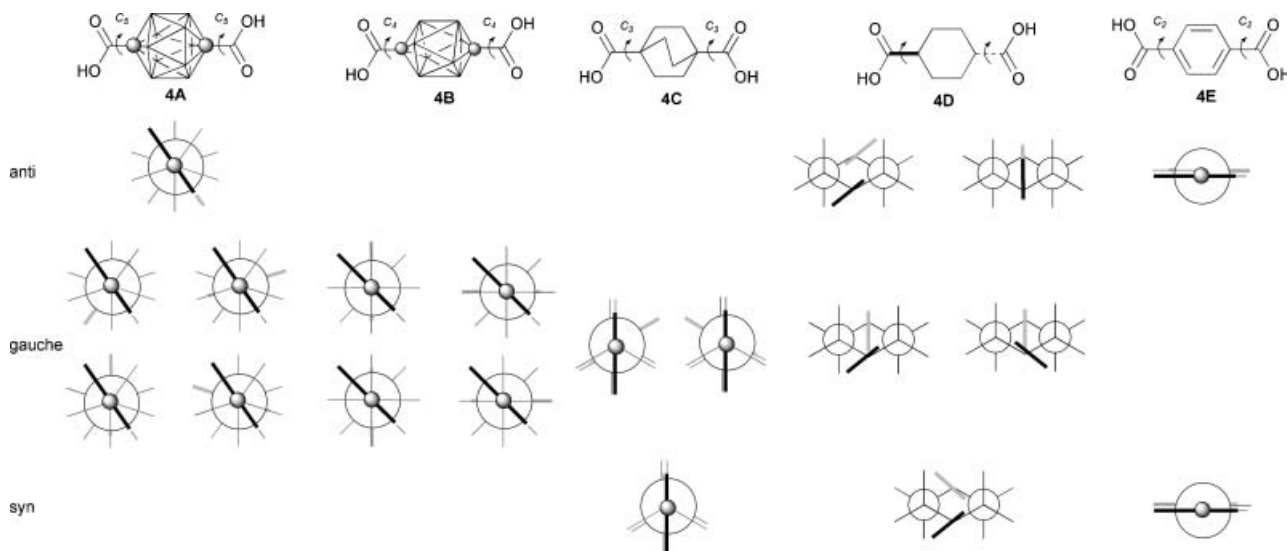


Figure 8. Possible relative orientations of two carboxyl groups in their ground states shown as bars in extended Newman projections along the long molecular axis of dicarboxylic acids **4**. The short end of the bar represents the C=O group and the long end the C–OH group.

derivative **4D** there are two gauche (an enantiomeric pair) in addition to two antiperiplanar rotamers and a pseudo synperiplanar rotamer. The diacid **4B** is unique among the five diacids **4**. The D_{4d} symmetry of the 10-vertex *p*-carborane (**B**) prevents the coplanar alignment of the carboxyl groups in the conformational ground state and all four rotamers are chiral (two pairs of enantiomers). This is particularly unfavourable for supporting the liquid crystalline state.

Thus, diacid **4E** has both conformers compatible with a liquid crystalline state, cyclohexane diacid **4D** has two out of five, bicyclo[2.2.2]octane **4C**, one out of three, 12-vertex *p*-carborane **4A** one out of five, and **4B** has none.

Molecular and crystal structures

Colourless orthorhombic crystals of **1A[3]**, monoclinic crystals of **1B[4]** and triclinic crystals of **1C[4]** were grown by slow evaporation of ethanol /CH₂Cl₂ solutions at ambient temperature, and their solid state structure were determined by X-ray diffraction (45). Selected geometrical parameters for **1A[3]**, **1B[4]** and **1C[4]** are listed in Table 5, and their molecular structures are shown in Figure 9.

Molecules of **1A[3]** are found to have C_i symmetry (Figure 9(a)). The carboxyl groups are nearly orthogonal to the benzene ring and adopt a staggered orientation with respect to the carborane cage. The observed B(3)–C–C=O dihedral angle is 20.1(3)°, and it corresponds to 35° calculated with the MP2 method

Table 5. Selected bond lengths (Å) and angles (°) for **1A[3]**, **1B[4]** and **1C[4]**.

	1A[3]		1B[4]		1C[4]	
Distances		molecule A	molecule B		molecule C	
C _{cage} –CO	1.514(3)	1.500(4) ^a	1.502(4) ^a		1.494(4) ^a	1.5115(30) ^a
X–C, ^b avrg	1.715(3)	1.606(4)	1.602(4)		1.601(4)	1.537(3)
B–B belt, avrg	1.785(3)	1.860(4)	1.851(5)		1.849(5)	na
B–B interbelt, avrg	1.764(3)	1.817(4)	1.812(4)		1.810(5)	na
C···C	3.075	3.354	3.355		3.355	2.606
Angles						
X–C–C=O ^b	20.1(3)	28.9(4), 30.7(4)	6.0(4), 36.4(5)		45.5(5), 45.2(4)	30.9(2), –5.4(3)
C _{Ph} –C _{Ph} –O–C _{alk}	3.3(3)	3.5(4), 6.6(4)	6.7(4), 12.8(6) or 16.5(5) ^c		0.3(4), 7.6(4)	4.7(2) 4(2) or –0.8(18) ^c
O–C=O, O–C=O ^d	0	16.5	2.4		46.3	80.1
O–C=O, Ph ^d	85.9	78.8, 62.6	76.9, 78.9		86.6, 58.0	66.9, 72.5
Ph, Ph ^d	0	3.2	5.3		10.1	60.0

^a Average of two values. ^b X=B for **1A[3]** and **1B[4]**, and X=C for **1C[4]**. ^c Positional disorder. ^d Angle between two planes. The benzene ring plane is defined by the three carbon atoms adjacent to the OOC group.

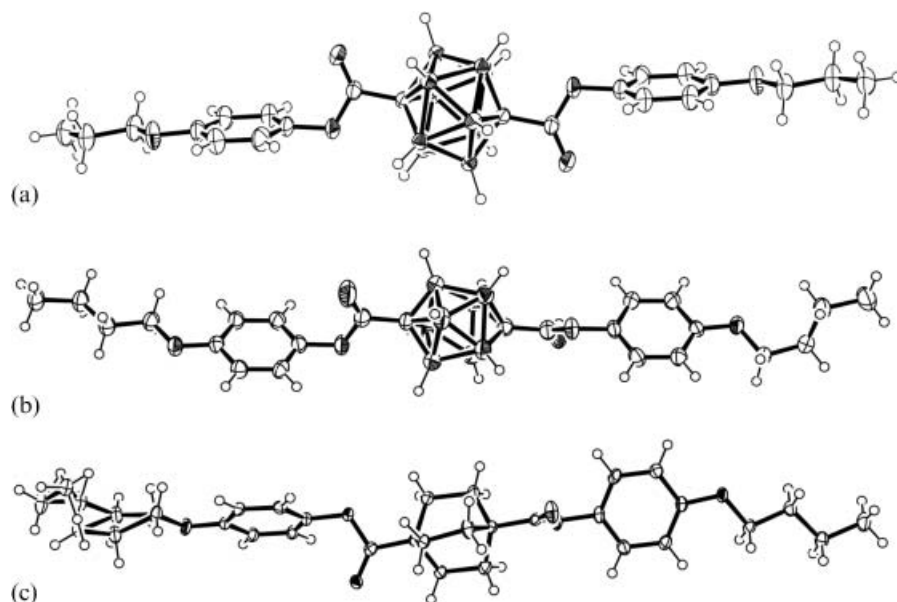


Figure 9. Thermal ellipsoid diagrams for (a) bis(4-propyloxyphenyl) 1,12-dicarba-*closo*-dodecaborane-1,12-dicarboxylate (**1A[3]**), b) bis(4-butoxyphenyl) 1,10-dicarba-*closo*-decaborane-1,10-dicarboxylate (**1B[4]**, molecule C), and c) bis(4-butoxyphenyl) bicyclo[2.2.2]octane-1,4-dicarboxylate (**1C[4]**), drawn at 50% probability. Selected bond lengths and angles are shown in Table 5.

as the global conformational minimum for 1,12- $C_2B_{10}H_{11}$ -1-COOH (**5A**, Table 4). The propyl chain adopts an almost ideal all-*trans* conformation ($176.9(2)^\circ$), and the propoxy group is nearly coplanar ($3.3(3)^\circ$) with the benzene ring. The interatomic distances and angles of the carborane cage are close to those reported recently for 1,12-dicarba-*closo*-dodecaborane-1,12-dicarbonitrile (**39**).

In contrast to **1A[3]**, molecules of both **1B[4]** and **1C[4]** show no molecular symmetry and one of the alkyl chains is disordered. Crystallographic analysis of **1B[4]** revealed three unique molecules in the asymmetric unit cell (Figure 9b). In molecules A and B one of the butyl chains adopts a gauche conformation around the $C_\alpha-C_\beta$ bond, and the other is in the nearly ideal all-*trans* conformation. In molecule B both butyl chains adopt the gauche conformation around the $C_\gamma-C_\delta$ bond, and one of the butyl groups is positionally disordered over two sites in an approximately 1:1 ratio of occupancy. In all three molecules the alkoxy oxygen atom is conjugated with the benzene ring, and the $C-O-C_{Ph}-C_{Ph}$ angle varies between $0.3(4)^\circ$ in molecule C and $16.5(5)^\circ$ in molecule B. There are two orientations of the carboxyl group in molecules A and C relative to the benzene ring, and the interplanar angles are about 60° and 80° , respectively. In contrast, both COO groups in molecule B form interplanar angles with the benzene ring close to 80° , but incidentally one of the butyl chains is disordered. Greater variations are observed in the

orientation of the carboxyl groups with respect to the boron cluster. Only in molecule C both carboxyl groups are nearly ideally staggered (Figure 9(b)), which is consistent with the calculated conformational minimum for acid 1,10- $C_2B_8H_9$ -1-COOH (**5B**, Table 4). Similar staggered orientation of the COO groups is observed in molecule A with the smaller dihedral angle of about 30° . In molecule B, however, one of the carboxyl groups adopts an orientation of only 6.0° short of the ideal eclipsed conformation, which, according to the calculations, represents a rotational transition state higher in energy than the GS by about 2 kcal mol^{-1} (Table 4). These variations in the COO group orientation relative to the boron cage and also to the benzene ring result in almost coplanar arrangement of the two benzene rings in each molecule. The resulting Ph-Ph interplanar angle varies from 10° in molecule C to as little as about 3° in molecule A, which is significantly less than the ideal 45° imposed by the cluster symmetry (Figure 8). The dimensions of the 10-vertex carborane cage in **1B[4]** are close to those recently reported for 1,10-dicarba-*closo*-decaborane-1,10-dicarbonitrile (**46**).

In a molecule of **1C[4]** one of the butyl chains is statistically disordered over two positions, while the other adopts a nearly ideal all-*trans* conformation (Figure 9(c)). The carboxyl groups adopt two orientations relative to the bicyclo[2.2.2]octane ring. One of the COO groups nearly eclipses the skeletal C-C bond and the experimental dihedral angle of $5.4(3)^\circ$

(Table 5) is consistent with 3.7° calculated for a conformational minimum in bicyclo[2.2.2]octane-1-carboxylic acid (**5C**, Table 4). The other carboxyl group is apparently forced out of the conformational minimum by the crystal packing forces and forms a 30.9° dihedral angle with the carbocycle. This is an intermediate position between the rotational ground state (3.7°) and rotational transition state (47°). In consequence, the carboxyl groups form an interplanar angle of 80.1° , which is nearly 40° lower than for the ideal gauche rotamer (Figure 8). The orientation of the carboxyl groups relative to their adjacent benzene rings is similar and both form interplanar angles of about 70° , which is a typical value for mesogenic phenyl benzoates (47). The C_3 symmetry of the bicyclo[2.2.2]octane ring results in a rather large interplanar angle of 60° between the two benzene rings.

The crystal packing of molecules **1A[3]** results in the arrangement of carborane cages in infinite two-dimensional sheets parallel to the a - b crystallographic plane and separated by about 31 \AA . The space between the "carborane planes" is filled with alternating aliphatic and aromatic groups. In contrast, boron clusters in the crystal of **1B[4]** are arranged into three molecule-wide infinite "carborane ribbons" parallel to the a - c crystallographic plane and propagating along the a axis. The neighbouring "carborane ribbons" are shifted relative to each other along the c axis by half of the inter-ribbon separation distance (about 15.5 \AA). In each "ribbon", the outer 10-vertex carborane cages belonging to molecules **A** and **C** weakly interact with the alkyl chains, while the benzene rings are aligned antiparallel to each other. The cages isolated in the interior of the "ribbon" are part of molecule **B** in which one of the butyl chains is positionally disordered.

In the crystals structure of **1C[4]** molecules form infinite molecular sheets parallel to the a - b plane with the molecules tilted to the plane.

3. Discussion

Behavior of the T_{NI} in homologous series has been investigated experimentally (48, 49) and theoretically (50, 51). In general, high-clearing temperature mesogens in homologous series exhibit descending trends and low-temperature mesogens ascending trends in T_{MI} with the characteristic alternating (even-odd) pattern. The existence of these two trends has been qualitatively explained as a balance between increasing polarisability anisotropy $\Delta\alpha$ and molecular flexibility with the increasing alkyl chain length in a

homologous series. This is expressed by de Jeu *et al.* (50) as

$$T_C = \frac{2A}{4.54k - 2B} \quad (3)$$

in which the quantity A is approximately proportional to $(\Delta\alpha)^2$, whereas the parameter B is related to the molecular shape anisotropy. Thus, at low temperatures the increase in $\Delta\alpha$ dominates and the T_C increases with increasing chain length. For high transition temperature mesogens however, thermally populated conformational states cause increasing deviation from a rod-like molecular shape. This is reflected in decreasing B (and also $\Delta\alpha$) and consequently decreasing T_C in a homologous series (52). Another way to describe this effect is that diminishing polar (dipolar and quadrupolar) interactions due to increasing molecular flexibility and mean intermolecular separation with the increasing chain length lead to decrease T_{NI} in a homologous series (17).

Nematic-isotropic transition temperatures in each homologous series of diesters **1A[n]**-**1E[n]** follow the typical descending and alternating pattern (48) approaching a constant value with increasing alkyl chain length (Figure 3). The series differ in the central fragment, which give rise to electronic [mainly parameter A in Equation (3)] and conformational [parameter B in Equation (3)] differences between the series. The latter conformational factor appears to be more important in affecting the phase stability in diesters **1**. Since variations in symmetry and conformational properties of the central structural units determine molecular flexibility, the effective molecular aspect ratio depends on the chain length. This, in turn, results in different trends in the parameter B [Equation (3)] with the increasing chain length, and consequently in different shape of the T_{MI} curve for each individual homologous series. Thus, variation in behaviour of the T_{MI} trend for homologous series can be linked to conformational properties of the central structural unit. Since parameters A and B have complex dependence on the chain length n , Equation (3) cannot be used for analysis of the homologous series. Instead, we used an empirical exponential function to approximate behaviour of the series for low and moderate n values ($n \leq 22$). This suggests a possibility of a detailed quantitative comparison of factors imparting stability of their mesophases.

Approximately constant value ΔT_{MI} for bicyclo[2.2.2]octanes **1C[n]** in Figure 4 suggests that the conformational factors in the bicyclo[2.2.2]octanes **1C[n]** are similar to those in the reference series of terephthalates **1E[n]**. In contrast, the ascending character of the ΔT_{MI} curve for cyclohexanes **1D[n]**

and descending trend for the ΔT_{MI} curve for carborane series **1A[n]** and **1B[n]** indicate that conformational properties of the central ring vary significantly from those of benzene and bicyclo[2.2.2]octane. This suggests that in the former, the effective molecular aspect ratio is steadily improving with longer alkyl chain, while in the carborane derivatives the effective molecular aspect ratio is systematically decreasing relative to that of the terephthalates **1E[n]**.

The rising ΔT_{MI} curve for **1D[n]** relative to terephthalates **1E[n]** in Figure 4 and the slope of 0.76 for the correlation in Figure 5 are consistent with the decreasing concentration of the non-mesogenic diaxial conformer (Figure 10) in higher homologues that have lower clearing temperatures. The clearing temperatures for the hypothetical pure diequatorial conformer **1D[n]-ee** can be estimated from the free energy difference ΔG between the diaxial and diequatorial conformers of **1D[n]**, and colligative properties of the clearing temperature. Thus, the observed clearing temperatures $T_{MI}(\mathbf{D})$ for series **1D[n]** can be expressed as

$$T_{MI}(\mathbf{D}) = T_{MI}(\mathbf{ee})(1-x) + T_{MI}(\mathbf{aa})x, \quad (4)$$

in which $T_{MI}(\mathbf{ee})$ and $T_{MI}(\mathbf{aa})$ are clearing temperatures for pure diequatorial (**1D[n]-ee**) and diaxial (**1D[n]-aa**) conformers, respectively, and x is mole fraction calculated from the steric energy, ΔG . The diaxial conformer is assumed to be non-mesogenic with $T_{MI}(\mathbf{aa})=0$ K (53). This leads to

$$\begin{aligned} T_{MI}(\mathbf{ee}) &= T_{MI}(\mathbf{D})(K+1) \\ &= T_{MI}(\mathbf{D})\left(e^{-\Delta G/RT_{MI}(\mathbf{D})} + 1\right), \end{aligned} \quad (5)$$

in which the mole fraction x is expressed using either the equilibrium constant K or free energy difference ΔG .

Figure 5 demonstrates that the $T_{NI}(\mathbf{D})$ values plotted against $T_{NI}(\mathbf{E})$ temperatures give a linear correlation with the slope $k=0.76$, while for bicyclo[2.2.2]octane diesters **1C[n]** the slope is $k=0.99$. If only the axial-equatorial conformational equilibrium

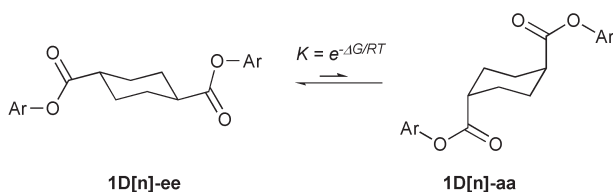


Figure 10. The equilibrium between the diequatorial and diaxial conformers of diesters **1D[n]**.

(Figure 10) is responsible for the inclining ΔT_{MI} curve for **1D[n]** in Figure 4, than for the pure diequatorial conformer **1D[n]-ee** the slope k for the plot of $T_{MI}(\mathbf{ee})$ vs $T_{MI}(\mathbf{E})$ is expected to be close to unity ($T_{MI}(\mathbf{ee})=T_{MI}(\mathbf{E}) \times 1+m$) and ΔT_{MI} approximately constant ($T_{MI}(\mathbf{ee}) - T_{MI}(\mathbf{E})=m$). To obtain slope $k=1.0$ for the correlation $T_{MI}(\mathbf{ee})$ vs $T_{MI}(\mathbf{E})$, the steric energy parameter ΔG in Equation (5) was set at $2.06 \text{ kcal mol}^{-1}$ (54), and the resulting plot is shown in Figure 11. The plot of the relative clearing temperature for the diequatorial conformer **1D[n]-ee** shown in Figure 12 is nearly flat resembling that of **1C[n]**, and the mean difference between the two sets of clearing temperatures, ΔT_{MI} , is $+32 \pm 2$ K (53).

The implied higher mesophase stability by 32 K for the diequatorial conformers **1D[n]-ee** than for terephthalates **1E[n]** is consistent with the generally higher T_{NI} for near-room temperature nematic phenyl cyclohexanecarboxylates than for their benzoate analogues. For instance, 4-alkoxyphenyl 4-pentylcyclohexanecarboxylates (**55**) have N-I transition temperatures in the range of 60°C to 85°C at which the concentration of the non-mesogenic diaxial conformer is low and can be estimated at about 1%. These clearing temperatures are higher than those for 4-alkoxyphenyl 4-pentylbenzoates (**56**) by an average of about 20 K.

The ΔG value of $2.06 \text{ kcal mol}^{-1}$ established in the fitting process is consistent with albeit smaller than the sum of two experimental (57) steric energies for the carboethoxy group of about $2.6 \text{ kcal mol}^{-1}$ in the temperature range of T_{MI} values for series **1D[n]**. The

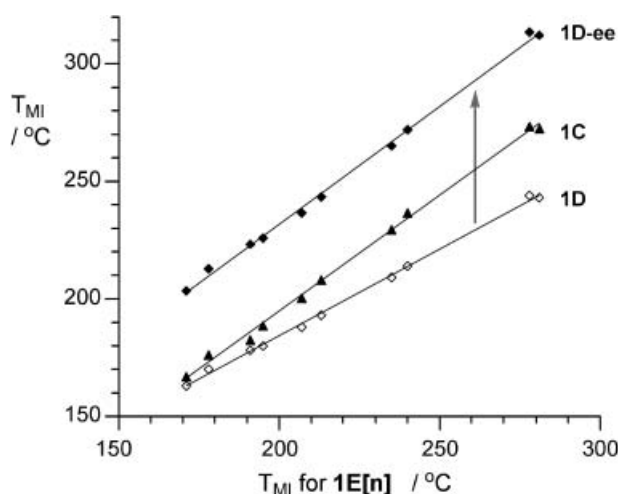


Figure 11. A plot of the T_{MI} for diesters **1D[n]** (open diamonds) and the diequatorial conformer **1D[n]-ee** (filled diamonds) vs T_{MI} of the terephthalates **1E[n]**. Best fit lines: **1D[n]**: $T_{MI}(\mathbf{D})=36.8+0.737T_{MI}(\mathbf{E})$; **1D[n]-ee**: $T_{MI}(\mathbf{ee})=31.0+1.00T_{MI}(\mathbf{E})$. $R^2=0.998$. Data for **1C[n]** (triangles) are shown for reference.

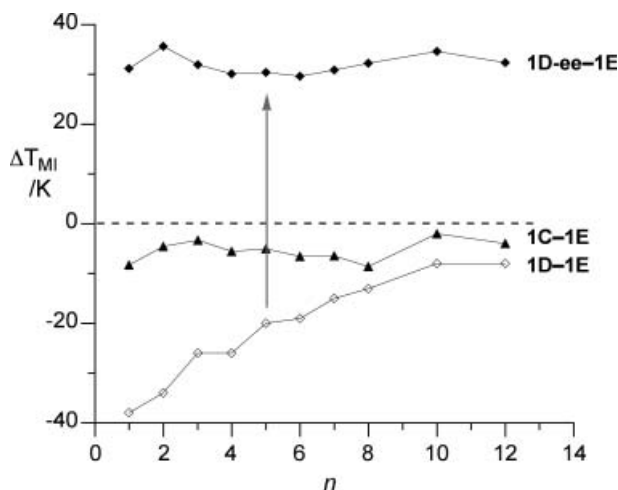


Figure 12. The T_{MI} for and **1D[n]** (open diamonds) and for diequatorial conformer **1D[n]-ee** (diamonds) relative to that of terephthalates **1E[n]** ($\Delta T_{MI} = T_{MI} - T_{MI}(E)$). Data for **1C[n]** (triangles) are shown for reference. The lines are guides for the eye.

difference of about $0.5 \text{ kcal mol}^{-1}$ between the two values is not unexpected, and non-additivity of the substituent steric energies is often observed in 1,4-disubstituted cyclohexanes (58–60).

The large decrease in the phase stability by nearly 50 K upon changing the orientation of the carboxyl group in the cyclohexane derivatives **1D[n]** and **2D[n]** (Figure 6) can be rationalised also using the axial-equatorial conformational equilibrium of the substituents on the cyclohexane ring (2). Since the steric energy value for the acetoxy group (61) is lower than that of the carboethoxy ($0.71 \text{ kcal mol}^{-1}$ vs. $1.3 \text{ kcal mol}^{-1}$) then much higher concentration of the non-mesogenic diaxial conformer and consequently lower dynamic aspect ratio is expected for dibenzoates **2D[n]** than for the dicarboxylates **1D[n]**. This unfavourable situation for the dibenzoates is compounded further by significant non-additivity of the steric parameter of the acyloxy group. Experiments demonstrated that the ΔG difference between the diequatorial and diaxial conformers of *trans*-1,4-diacetyloxycyclohexane ranges from $0.16 \text{ kcal mol}^{-1}$ in acetone (59) to $0.41 \text{ kcal mol}^{-1}$ in CCl_4 (60), which are more than 1 kcal mol^{-1} less than the sum of two individual steric energies for the AcO group (61) ($1.42 \text{ kcal mol}^{-1}$). In contrast, the change of the orientation of the COO group in bicyclo[2.2.2]octanes or benzenes has significantly smaller effect on the clearing temperatures (Figure 6), since the overall molecular conformations are essentially the same.

The explanation of the shape of the ΔT_{NI} curve for the carborane series **1A[n]** and **1B[n]** in Figure 4 requires a different approach and consideration of

molecular symmetry of the *p*-carboranes and conformational properties of their carboxyl derivatives.

Inspection of Figure 8 shows that substituents in all five dicarboxylic acids (and their esters) can adopt 2–5 relative orientations that are determined by the rotational symmetry of the structural units A–E. Also, the increasing number of available conformational minima (the number of rotamers) in the series E→A is paralleled by the decreasing barrier to the internal rotation around the A–COOH bond from $\Delta G_{298}^\ddagger = 6.75 \text{ kcal mol}^{-1}$ in **5E** to $\Delta G_{298}^\ddagger = 1.2 \text{ kcal mol}^{-1}$ in **5A** (Table 4). The latter value is entirely due to entropy change in the rotational transitional state, and is the lowest in the molecule of diester **1A[n]**. This indicates that for 12-vertex *p*-carborane derivatives the internal rotation involving the A–COOH bond is particularly easy; it is the most frequent and leads to the largest number of rotamers. Consequently, this significantly less restricted rotation around the C–C bond gives rise to a rotational cone curved by the alkoxyaryl group, as shown in Figure 13. Since the length of the alkyl chain increases in the homologous series, so does the size of the cone. This leads to the diminishing effective molecular aspect ratio of the diesters, and, in consequence, progressively lower clearing temperatures relative to terephthalates **1E[n]**.

Figure 8 also shows that with the exception of the 10-vertex *p*-carborane (**B**) all structural units can support coplanar or nearly co-planar orientation of the antipodal substituents. In derivatives of 12-vertex *p*-carborane (**A**), cyclohexane (**D**) and benzene (**E**) the substituents can adopt antiperiplanar orientations, whereas in bicyclo[2.2.2]octane (**C**) only a nearly synperiplanar conformation is possible. This is supported by crystallographic studies for terephthalate (62) and cyclohexane-1,4-dicarboxylate mesogens (43) and those reported here for **1A[3]**, which show antiperiplanar arrangement of the carboxyl substituents. Such conformations give rise to the most elongated molecular shapes and are particularly favourable for supporting of mesophases. In contrast, the carboxyl groups in derivatives of 10-vertex *p*-carborane **B** cannot adopt coplanar alignment in the conformational ground state. Instead, the substituent planes form an angle of 45° and all conformers are



Figure 13. Least restricted rotation around the C–C(=O) bond results in a cone curved by the alkoxyphenyl groups in **1A[n]**.

chiral. This is supported by solid-state structures of **1B[4]** and four other derivatives of *p*-carborane **B** (5, 13) and also another 10-vertex cluster (63), in which alkyl chains are frequently exhibit positional disorder and are forced to gauche conformations by crystal packing forces. For instance, in the structure of **1B[4]** the approximate coplanarity of the 4-alkoxyphenyl fragments in molecules **A** and **B** is achieved by changing the optimum torsional angles between the COO group and the *p*-carborane cage and the COO group and the benzene ring (Table 5). The non-coplanar orientation of the substituents in derivatives of *p*-carborane **B** in the conformational ground state results in progressively less favourable effective molecular aspect ratio with the increasing alkyl chain length in a homologous series. Thus a combination of the necessarily angular relative orientation of the antipodal substituents and the high number of conformational minima **1B[n]** give rise to progressively less favourable aspect ratio and consequently lower clearing temperatures relative to the terephthalates **1E[n]** in a homologous series.

The solid-state structure of the bicyclo[2.2.2]octane derivative **1C[4]** demonstrates also the difficulties with synperiplanar arrangement of the carboxyl group, which would lead to a bow-like molecular shape. Such a shape is disfavoured in the solid state and one or both substituents adopt less optimum orientation with respect to the carbocyclic ring. This is evident from analysis in Figure 9(c) and Table 5, and also from crystallographic studies of bicyclo[2.2.2]octane-1,4-dicarboxylic acid (**4C**) (64). In the structure of **4C**, the two carboxyl groups achieve the antiperiplanar arrangement by adopting staggered orientation that is about 25° off the global minimum or nearly 20° away from the calculated rotational transition state.

Conformational mobility and low dynamic molecular anisotropy can also be used to rationalise the exclusively nematic behaviour observed in both 12- and 10-vertex *p*-carborane derivatives **1A[n]** and **1B[n]** and in most other carborane-containing mesogens (5, 9–13). A similar lack of smectic properties in cyclohexane-1,4-diol dibenzoates **2D[n]** up to at least $n=12$ (35, 65) has been attributed to the excessive conformational flexibility of the 1,4-diacetoxycyclohexane (*vide supra*). Since the two conformers, diequatorial and diaxial, undergo fast interconversion, the average aspect ratio for the molecule is low, which is reflected in destabilisation of the smectic phase and mesophases in general. This argument can be extended to the carborane derivatives in which the extensive rotational mobility is incompatible with molecular packing in the smectic layers. The lack of smectic phases in the 10-vertex *p*-carborane derivatives can be ascribed, in part, to unfavourable

molecular shape originating from the symmetry of the carborane ring (D_{4d}), and in part to increased molecular flexibility and relatively large size of the carborane ring. These rationales are consistent with the generally observed stronger destabilisation of smectic than nematic phases by lowering molecular anisotropy with non-polar lateral substituents (48). Finally, the postulated conformational origin of the preferential destabilisation of the smectic phases is consistent with the relatively large entropy change at the clearing point for the carborane derivatives as compared with the hydrocarbon analogues. This suggests large conformational changes between the nematic and isotropic phases due to less restricted rotations around the \mathcal{A} -CO bonds and the gauche conformation in the 10-vertex *p*-carborane derivatives.

4. Summary and conclusions

Detailed investigation of five isostructural series of diesters **1A[n]**–**1E[n]** revealed significant differences in their mesogenic behaviour and phase stabilities. The effectiveness of the central structural unit in the diesters, and the impact of its symmetry and conformational properties on the mesophase stability was assessed by two types of numerical analysis of each series of mesogens: approximation of the clearing temperatures T_{MI} with an exponential function, and comparative studies using the terephthalates **1E[n]** as the reference.

Numerical analysis of the T_{MI} values for each series (n =even) using an empirical three-parameter exponential function gave limiting values $T_{MI}(\infty)$, which describes the ability of the structural element to stabilise the mesophase. The carbocyclic derivatives **1C[n]**–**1E[n]** asymptotically approach the limit $T_{MI}(\infty)$ of about 125°C, whereas the limit for the diesters containing carboranes **A** and **B** is 70°C and 49°C, respectively. The established effectiveness of the structural units follows the order: $C \sim D \sim E > A > B$. The results also demonstrate that the exponential function can be used for the modelling of a combination of the N-I and SmA-I transition temperatures.

The second numerical analysis used the T_{MI} values for terephthalates **1E[n]** as the reference and revealed three different types of behaviour for remaining four series of diesters: similar mesophase stability (bicyclo[2.2.2]octanes **1C[n]**), increasing mesophase stability (cyclohexanes **1D[n]**) and decreasing mesophase stability (carboranes **1A[n]** and **1B[n]**) relative to $T_{MI}(E)$ with increasing length of the alkyl chain. This is evident from the trends in the plots of $\Delta T_{MI}(n)$ and slopes in linear correlations of T_{MI} vs. $T_{MI}(E)$. The observed differences were ascribed to the dynamic molecular aspect ratio and

molecular flexibility, which result from conformational properties of the cyclohexane (**D**) and symmetry of the *p*-carboranes (**A** and **B**). Thus, a steady decrease of the relative phase stability in the carborane series **1A[n]** and **1B[n]** is a consequence of the high number of rotamers in both and lack of coplanar arrangements of substituents in derivatives of **B**. Also the exclusively nematogenic behaviour of the carborane derivatives was ascribed to molecular flexibility of 12-vertex and molecular shape of 10-vertex derivatives.

Overall, the presented numerical analysis provides a sensitive test for internal-consistency of the thermal data and purity of the compounds. It also serves as a convenient and very useful tool for comparative investigation of series of closely related mesogens and for predicting clearing temperatures of unknown homologues.

5. Experimental

General methods

¹H NMR spectra were obtained at 300 MHz in CDCl₃ and referenced to TMS unless stated otherwise. Elemental analysis was provided by Atlantic Microlab, GA, or Instrumental Analysis Center for Chemistry, Graduate School of Science, Tohoku University. 10- and 12-vertex *p*-carboranes were purchased from Katchem s.r.o. (Prague, Czech Republic). Other chemicals were purchased from Aldrich or Tokyo Kasei Ltd.

Optical microscopy and phase identification was performed using a PZO "Biolar" polarising microscope equipped with a HCS 402 Instec hot stage. Thermal analysis was obtained using a TA Instruments 2920 DSC. Transition temperatures (onset) and enthalpies were obtained using small samples (1–2 mg) and a heating rate of 5 K min⁻¹ under a flow of nitrogen gas. The clearing transition was typically less than 0.3 K wide.

Synthesis

Preparation of esters – general procedures.

In Method A, a suspension of *p*-carborane-1,12-dicarboxylic acid (**19**) (116 mg, 0.5 mmol) or *p*-carborane-1,10-dicarboxylic acid (**20**) (105 mg, 0.5 mmol) and PCl₅ (218 mg, 1.05 mmol) in dry benzene (2 ml) was stirred at 40–50°C until all dissolved. After additional 15 min of stirring, the solvent and POCl₃ were removed under reduced pressure. Alternatively, *p*-carborane-1,12-dicarboxylic acid (0.5 mmol) was converted (rt, 2 h) to the acid chloride using oxalyl chloride (0.2 ml) in CH₂Cl₂ (2 ml) containing a drop of DMF.

The resulting crude acid chloride was dissolved in dry CH₂Cl₂ or toluene (2 ml), phenol (1.0 mmol) was added followed by dry pyridine (0.10 ml). The mixture was stirred at ambient temperature for 3 h, passed through a silica gel plug, washed with CH₂Cl₂ and the eluent evaporated. The residue was passed through a silica gel column (CH₂Cl₂ or 1:10 AcOEt/hexane) and recrystallised (typically isooctane/toluene or CH₂Cl₂/MeOH).

Final purification for analysis was performed as follows. Each compound was dissolved in CH₂Cl₂, solution filtered through cotton to remove particles, evaporated and the product recrystallised from the indicated solvent until constant temperature. The resulting crystals were dried in vacuum overnight at ambient temperature. The purity was confirmed by combustion analysis.

In Method B, a suspension of bicyclo[2.2.2]octane-1,4-dicarboxylic acid (94 mg, 0.5 mmol) and PCl₅ (218 mg, 1.05 mmol) in POCl₃ (0.5 ml) was stirred and gently refluxed until all dissolved. After additional 15 min of stirring, POCl₃ was removed under reduced pressure. The resulting crude acid chloride was dissolved in dry CCl₄ (2 ml), phenol (1.0 mmol) was added and the mixture was refluxed overnight. Upon cooling, the mixture was passed through a silica gel plug, washed with CH₂Cl₂ and the eluent evaporated. The resulting crude product was purified as described in Method A.

Bis(4-methoxyphenyl) 1,12-dicarba-closo-dodecaborane-1,12-dicarboxylate (1A[1]).

From EtOH/AcOEt, ¹H NMR: δ 1.5–4.0 (br m, 10H), 3.78 (s, 6H), 6.81 and 6.89 (AA'BB', *J*=9.3 Hz, 8H). Elemental analysis: calculated for C₁₈H₂₄B₁₀O₆, C 48.64, H 5.44; found, C 49.01, H 5.41%.

Bis(4-ethoxyphenyl) 1,12-dicarba-closo-dodecaborane-1,12-dicarboxylate (1A[2]).

From isooctane/toluene, ¹H NMR: δ 1.39 (t, *J*=7.0 Hz, 6H), 1.5–4.0 (br m, 10H), 3.99 (q, *J*=7.0 Hz, 4H), 6.82 and 6.87 (AA'BB', *J*=9.4 Hz, 8H). Elemental analysis: calculated for C₂₀H₂₈B₁₀O₆, C 50.84, H 5.97; found, C 51.37, H 6.07%.

Bis(4-propoxyphenyl) 1,12-dicarba-closo-dodecaborane-1,12-dicarboxylate (1A[3]).

From isooctane/toluene, ¹H NMR: δ 1.02 (t, *J*=7.4 Hz, 6H), 1.5–4.0 (br m, 10H), 1.78 (sextet, *J*=7.0 Hz, 4H), 3.87 (t, *J*=6.5 Hz, 4H), 6.83 and 6.87 (AA'BB', *J*=9.4 Hz, 8H). Elemental analysis: calculated for C₂₂H₃₂B₁₀O₆, C 52.79, H 6.44; found, C 52.88, H 6.45%.

Bis(4-pentyloxyphenyl) 1,12-dicarba-closo-dodecaborane-1,12-dicarboxylate (1A[5]).

From isooctane, ^1H NMR (270 MHz): δ 0.92 (t, $J=6.8$ Hz, 6H), 1.30–1.50 (m, 8H), 1.5–4.0 (br m, 10H), 1.76 (quint, $J=6.6$ Hz, 4H), 3.90 (t, $J=6.6$ Hz, 4H), 6.82 and 6.87 (AA'BB', $J=9.1$ Hz, 8H). Elemental analysis: calculated for $\text{C}_{26}\text{H}_{40}\text{B}_{10}\text{O}_6$, C 56.09, H 7.24; found, C 55.80, H 7.48%.

Bis(4-hexyloxyphenyl) 1,12-dicarba-closo-dodecaborane-1,12-dicarboxylate (1A[6]).

From hexane, ^1H NMR (270 MHz): δ 0.90 (t, $J=6.8$ Hz, 6H), 1.25–1.50 (m, 12 H), 1.5–4.0 (br m, 10H), 1.75 (quint, $J=6.6$ Hz, 4H), 3.90 (t, $J=6.6$ Hz, 4H), 6.82 and 6.87 (AA'BB', $J=9.1$ Hz, 8H). Elemental analysis: calculated for $\text{C}_{28}\text{H}_{44}\text{B}_{10}\text{O}_6$, C 57.51, H 7.58; found, C 57.50, H 7.71%.

Bis(4-heptyloxyphenyl) 1,12-dicarba-closo-dodecaborane-1,12-dicarboxylate (1A[7]).

From hexane, ^1H NMR (270 MHz): δ 0.89 (t, $J=6.8$ Hz, 6H), 1.20–1.50 (m, 16H), 1.5–4.0 (br m, 10H), 1.75 (quint, $J=6.6$ Hz, 4H), 3.90 (t, $J=6.6$ Hz, 4H), 6.82 and 6.87 (AA'BB', $J=9.2$ Hz, 8H). Elemental analysis: calculated for $\text{C}_{30}\text{H}_{48}\text{B}_{10}\text{O}_6$, C 58.80, H 7.89; found, C 58.62, H 8.10.

Bis(4-octyloxyphenyl) 1,12-dicarba-closo-dodecaborane-1,12-dicarboxylate (1A[8]).

From pentane, ^1H NMR: δ 0.88 (t, $J=6.8$ Hz, 6H), 1.25–1.49 (m, 20H), 1.5–4.0 (br m, 10H), 1.75 (quint, $J=7.0$ Hz, 4H), 3.90 (t, $J=6.6$ Hz, 4H), 6.82 and 6.87 (AA'BB', $J=9.4$ Hz, 8H). Elemental analysis: calculated for $\text{C}_{32}\text{H}_{52}\text{B}_{10}\text{O}_6$, C 59.97, H 8.18. Found, C 60.23, H 8.22%.

Bis(4-nonyloxyphenyl) 1,12-dicarba-closo-dodecaborane-1,12-dicarboxylate (1A[9]).

From hexane, ^1H NMR: δ 0.88 (t, $J=6.7$ Hz, 6H), 1.27–1.44 (m, 24), 1.5–4.0 (br m, 10H), 1.75 (quint, $J=7.0$ Hz, 4H), 3.90 (t, $J=6.6$ Hz, 4H), 6.82 and 6.87 (AA'BB', $J=9.3$ Hz, 8H). Elemental analysis: calculated for $\text{C}_{34}\text{H}_{56}\text{B}_{10}\text{O}_6$, C 61.05, H 8.44; found, C 60.98, H 8.43%.

Bis(4-decyloxyphenyl) 1,12-dicarba-closo-dodecaborane-1,12-dicarboxylate (1A[10]).

From EtOH, MeCN or hexane, ^1H NMR: δ 0.88 (t, $J=6.9$ Hz, 6H), 1.24–1.37 (m, 24H), 1.39–1.48 (m, 4H), 1.5–4.0 (br m, 10H), 1.75 (quint, $J=7.1$ Hz, 4H), 3.89 (t, $J=6.6$ Hz, 4H), 6.75 and 6.77 (AA'BB', $J=9.1$ Hz, 8H). Elemental analysis: calculated for

$\text{C}_{36}\text{H}_{60}\text{B}_{10}\text{O}_6$, C 62.04, H 8.68; found, C 62.51, H 8.80%.

Bis(4-dodecyloxyphenyl) 1,12-dicarba-closo-dodecaborane-1,12-dicarboxylate (1A[12]).

From AcOEt, ^1H NMR (270 MHz): δ 0.88 (t, $J=7.3$ Hz, 6H), 1.20–1.50 (m, 36H), 1.5–4.0 (br m, 10H), 1.74 (quint, $J=6.8$ Hz, 4H), 3.90 (t, $J=6.7$ Hz, 4H), 6.82 (d, $J=9.7$ Hz, 4H), 6.87 (d, $J=8.9$ Hz, 4H). MS (EI): m/z 753 (M^+), 57 (100). Elemental analysis: calculated for $\text{C}_{40}\text{H}_{68}\text{B}_{10}\text{O}_6$, C 63.80, H 9.10; found, C 63.70, H, 8.81%.

Bis(4-tetradecyloxyphenyl) 1,12-dicarba-closo-dodecaborane-1,12-dicarboxylate (1A[14]).

From AcOEt, ^1H NMR (270 MHz): δ 0.88 (t, $J=6.9$ Hz, 6H), 1.20–1.50 (m, 44H), 1.5–4.0 (br m, 10H), 1.75 (quint, $J=6.6$ Hz, 4H), 3.90 (t, $J=6.6$ Hz, 4H), 6.82 (d, $J=9.6$ Hz, 4H), 6.87 (d, $J=9.4$ Hz, 4H). MS (FAB): m/z 810 ($\text{M}+1$), 307 (100). Elemental analysis: calculated for $\text{C}_{44}\text{H}_{76}\text{B}_{10}\text{O}_6$, C 65.31, H 9.47; found, C 65.69, H 9.38%.

Bis(4-hexadecyloxyphenyl) 1,12-dicarba-closo-dodecaborane-1,12-dicarboxylate (1A[16]).

From AcOEt, ^1H NMR (270 MHz): δ 0.88 (t, $J=7.1$ Hz, 6H), 1.20–1.50 (m, 52H), 1.5–4.0 (br m, 10H), 1.72 (quint, $J=6.6$ Hz, 4H), 3.90 (t, $J=6.6$ Hz, 4H), 6.82 (d, $J=9.6$ Hz, 4H), 6.87 (d, $J=9.1$ Hz, 4H). MS (FAB): m/z 866 ($\text{M}+1$), 137 (100 %). Elemental analysis: calculated for $\text{C}_{48}\text{H}_{84}\text{B}_{10}\text{O}_6$, C 66.63, H 9.78; found, C 66.68, H 9.95%.

Bis(4-octadecyloxyphenyl) 1,12-dicarba-closo-dodecaborane-1,12-dicarboxylate (1A[18]).

From AcOEt, ^1H NMR (400 MHz): δ 0.88 (t, $J=6.9$ Hz, 6H), 1.20–1.40 (m, 56H), 1.42 (quint, $J=6.9$ Hz, 4H), 1.5–4.0 (br m, 10H), 1.75 (quint, $J=6.8$ Hz, 4H), 3.90 (t, $J=6.6$ Hz, 4H), 6.82 (d, $J=9.3$ Hz, 4H), 6.87 (d, $J=9.3$ Hz, 4H). MS (FAB): m/z 922 ($\text{M}+1$), 166 (100). Elemental analysis: calculated for $\text{C}_{52}\text{H}_{92}\text{B}_{10}\text{O}_6$, C 67.78, H 10.06; found, C 67.79, H 10.09%.

Bis(4-eicosyloxyphenyl) 1,12-dicarba-closo-dodecaborane-1,12-dicarboxylate (1A[20]).

From AcOEt, ^1H NMR (270 MHz): δ 0.88 (t, $J=7.0$ Hz, 6H), 1.20–1.50 (m, 68H), 1.5–4.0 (br m, 10H), 1.75 (quint, $J=6.9$ Hz, 4H), 3.90 (t, $J=6.6$ Hz, 4H), 6.82 (d, $J=9.6$ Hz, 4H), 6.87 (d, $J=9.2$ Hz, 4H).

MS (FAB): m/z 978 (M+1), 155 (100). Elemental analysis: calculated for $C_{56}H_{100}B_{10}O_6$, C 68.81, H 10.31; found, C 68.84, H 10.38%.

Bis(4-docosyloxyphenyl) 1,12-dicarba-closo-dodecaborane-1,12-dicarboxylate (1A[22]).

From AcOEt, 1H NMR (400 MHz): δ 0.88 (t, $J=7.1$ Hz, 6H), 1.20–1.40 (m, 72H), 1.42 (quint, $J=6.7$ Hz, 4H), 1.5–4.0 (br m, 10H), 1.75 (quint, $J=7.0$ Hz, 4H), 3.90 (t, $J=6.6$ Hz, 4H), 6.82 (d, $J=9.3$ Hz, 4H), 6.87 (d, $J=9.3$ Hz, 4H). MS (FAB): m/z 1034 (M+1), 164 (100 %). Elemental analysis: calculated for $C_{60}H_{108}B_{10}O_6$, C 69.72, H 10.53; found, C 69.95, H 10.59%.

Bis(4-methoxyphenyl) 1,10-dicarba-closo-decaborane-1,10-dicarboxylate (1B[1]).

From isooctane/toluene, 1H NMR: δ 1.5–4.0 (br m, 8H), 3.85 (s, 6H), 6.98 (d, $J=9.1$ Hz, 4H), 7.25 (d, $J=9.1$ Hz, 4H). Elemental analysis: calculated for $C_{18}H_{22}B_8O_6$, C 51.37, H 5.27; found, C 51.57, H 5.23%.

Bis(4-ethoxyphenyl) 1,10-dicarba-closo-decaborane-1,10-dicarboxylate (1B[2]).

From isooctane/toluene, 1H NMR: δ 1.44 (t, $J=7.0$ Hz, 6H), 4.06 (q, $J=7.0$, 4H), 6.96 (d, $J=9.1$ Hz, 4H), 7.23 (d, $J=9.1$ Hz, 4H). Elemental analysis: calculated for $C_{20}H_{26}B_8O_6$, C 53.51, H 5.84; found, C 53.74, H 5.82%.

Bis(4-propoxyphenyl) 1,10-dicarba-closo-decaborane-1,10-dicarboxylate (1B[4]).

From isooctane, 1H NMR: δ 1.06 (t, $J=7.4$ Hz, 6H), 1.5–4.0 (br m, 8H), 1.83 (sextet, $J=7.1$ Hz, 4H), 3.95 (t, $J=6.6$, 4H), 6.97 (d, $J=9.1$ Hz, 4H), 7.22 (d, $J=9.1$ Hz, 4H). Elemental analysis: calculated for $C_{22}H_{30}B_8O_6$, C 55.40, H 6.34; found, C 55.28, H 6.33%.

Bis(4-butoxyphenyl) 1,10-dicarba-closo-decaborane-1,10-dicarboxylate (1B[5]).

From isooctane, 1H NMR (C_6D_6): δ 0.85 (t, $J=7.4$ Hz, 6H), 1.34 (sextet, $J=7.4$ Hz, 4H), 1.5–4.0 (br m, 8H), 1.56 (quint, $J=6.9$ Hz, 4H), 3.54 (t, $J=6.4$, 4H), 6.74 (d, $J=9.0$ Hz, 4H), 7.10 (d, $J=9.0$ Hz, 4H). ^{13}C NMR (C_6D_6): δ 14.0, 19.5, 31.6, 68.0, 115.4, 117.1 (br), 144.7, 157.8, 162.9. ^{11}B NMR (C_6D_6): δ -10.3 (d, $J=184$ Hz). Elemental analysis: calculated for $C_{24}H_{34}B_8O_6$, C 57.08, H 6.79; found, C 56.96, H 6.80%.

Bis(4-pentyloxyphenyl) 1,10-dicarba-closo-decaborane-1,10-dicarboxylate (1B[5]).

From isooctane, 1H NMR: δ 0.95 (t, $J=7.1$ Hz, 6H), 1.33–1.48 (m, 8H), 1.5–4.0 (br m, 8H), 1.81 (quint, $J=7.0$, 4H), 3.98 (t, $J=6.6$ Hz, 4H), 6.96 (d, $J=9.1$ Hz, 4H), 7.22 (d, $J=9.1$ Hz, 4H). Elemental analysis: calculated for $C_{26}H_{38}B_8O_6$, C 58.58, H 7.19; found, C 58.66, H 7.27%.

Bis(4-hexyloxyphenyl) 1,10-dicarba-closo-decaborane-1,10-dicarboxylate (1B[6]).

From isooctane and pentane, 1H NMR: δ 0.92 (t, $J=7.0$ Hz, 6H), 1.32–1.50 (m, 12H), 1.5–4.0 (br m, 8H), 1.80 (quint, $J=7.0$ Hz, 4H), 3.98 (t, $J=6.5$ Hz, 4H), 6.96 (d, $J=9.1$ Hz, 4H), 7.22 (d, $J=9.1$ Hz, 4H). Elemental analysis: calculated for $C_{28}H_{42}B_8O_6$, C 59.94, H 7.54; found, C 60.03, H 7.63%.

Bis(4-heptyloxyphenyl) 1,10-dicarba-closo-decaborane-1,10-dicarboxylate (1B[7]).

From hexane, 1H NMR: δ 0.90 (t, $J=6.7$ Hz, 6H), 1.25–1.49 (m, 16H), 1.5–4.0 (br m, 8H), 1.80 (quint, $J=7.0$ Hz, 4H), 3.98 (t, $J=6.5$ Hz, 4H), 6.97 (d, $J=9.1$ Hz, 4H), 7.22 (d, $J=9.1$ Hz, 4H). Elemental analysis: calculated for $C_{30}H_{46}B_8O_6$, C 61.16, H 7.87; found, C 61.22, H 7.96%.

Bis(4-octyloxyphenyl) 1,10-dicarba-closo-decaborane-1,10-dicarboxylate (1B[8]).

From pentane, 1H NMR: δ 0.90 (t, $J=6.7$ Hz, 6H), 1.25–1.49 (m, 20H), 1.5–4.0 (br m, 8H), 1.80 (quint, $J=7.0$ Hz, 4H), 3.98 (t, $J=6.5$ Hz, 4H), 6.96 (d, $J=9.1$ Hz, 4H), 7.22 (d, $J=9.1$ Hz, 4H). Elemental analysis: calculated for $C_{32}H_{50}B_8O_6$, C 62.27, H 8.17; found, C 62.53, H 8.17%.

Bis(4-nonyloxyphenyl) 1,10-dicarba-closo-decaborane-1,10-dicarboxylate (1B[9]).

From hexane, 1H NMR: δ 0.89 (t, $J=7.0$ Hz, 6H), 1.25–1.38 (m, 20H), 1.44–1.50 (m, 4H), 1.5–4.0 (br m, 8H), 1.80 (quint, $J=6.7$ Hz, 4H), 3.98 (t, $J=6.6$ Hz, 4H), 6.96 (d, $J=9.1$ Hz, 4H), 7.22 (d, $J=9.1$ Hz, 4H). Elemental analysis: calculated for $C_{34}H_{54}B_8O_6$, C 63.29, H 8.43; found, C 63.47, H 8.55%.

Bis(4-decyloxyphenyl) 1,10-dicarba-closo-decaborane-1,10-dicarboxylate (1B[10]).

From pentane, 1H NMR: δ 0.89 (t, $J=6.9$ Hz, 6H), 1.25–1.39 (m, 24H), 1.41–1.52 (m, 4H), 1.5–4.0 (br m, 8H), 1.80 (quint, $J=7.8$ Hz, 4H), 3.98 (t, $J=6.6$ Hz, 4H), 6.96 (d, $J=9.0$ Hz, 4H), 7.22 (d, $J=9.0$ Hz, 4H).

Elemental analysis: calculated for $C_{36}H_{58}B_8O_6$, C 64.22, H 8.68; found, C 64.49, H 8.72%.

Bis(4-dodecyloxyphenyl) 1,10-dicarba-closo-decaborane-1,10-dicarboxylate (1B[10]).

From hexane followed by MeCN, 1H NMR: δ 0.88 (t, $J=6.6$ Hz, 6H), 1.25–1.39 (m, 32H), 1.41–1.52 (m, 4H), 1.5–4.0 (br m, 8H), 1.80 (quint, $J=7.1$ Hz, 4H), 3.98 (t, $J=6.5$ Hz, 4H), 6.96 (d, $J=9.1$ Hz, 4H), 7.22 (d, $J=9.0$ Hz, 4H). Elemental analysis: calculated for $C_{40}H_{66}B_8O_6$, C 65.86, H 9.12; found, C 66.05, H 9.12%.

Bis(4-methoxyphenyl) bicyclo[2.2.2]octane-1,4-dicarboxylate (17) (1C[1]).

From isooctane/toluene, 1H NMR: δ 2.04 (s, 12H), 3.80 (s, 6H), 6.88 and 6.95 (AA'BB', $J=9.2$ Hz, 8H).

Bis(4-ethoxyphenyl) bicyclo[2.2.2]octane-1,4-dicarboxylate (1C[2]).

From isooctane/toluene, 1H NMR: δ 1.41 (t, $J=7.0$ Hz, 6H), 2.03 (s, 12H), 4.01 (q, $J=7.0$, 4H), 6.87 and 6.94 (AA'BB', $J=9.1$ Hz, 8H). Elemental analysis: calculated for $C_{26}H_{30}O_6$, C 71.21, H 6.90; found, C 71.37, H 6.95%.

Bis(4-propoxyphenyl) bicyclo[2.2.2]octane-1,4-dicarboxylate (1C[3]).

From isooctane/toluene, 1H NMR: δ 1.03 (t, $J=7.4$ Hz, 6H), 1.80 (sextet, $J=7.0$ Hz, 4H), 2.03 (s, 12H), 3.94 (t, $J=6.5$, 4H), 6.87 and 6.94 (AA'BB', $J=9.2$ Hz, 8H). Elemental analysis: calculated for $C_{28}H_{34}O_6$, C 72.08, H 7.35; found, C 71.86, H 7.32%.

Bis(4-butyloxyphenyl) bicyclo[2.2.2]octane-1,4-dicarboxylate (1C[4]).

From hexane, 1H NMR: δ 0.97 (t, $J=7.4$ Hz, 6H), 1.38–1.56 (m, 4H), 1.71–1.80 (m, 4H), 2.03 (s, 12H), 3.90 (t, $J=6.6$, 4H), 6.87 and 6.94 (AA'BB', $J=9.2$ Hz, 8H). Elemental analysis: calculated for $C_{30}H_{38}O_6$, C 72.85, H 7.74; found, C 72.82, H 7.81%.

Bis(4-pentyloxyphenyl) bicyclo[2.2.2]octane-1,4-dicarboxylate (1C[5]).

From hexane, 1H NMR (400 MHz): δ 0.93 (t, $J=7.1$ Hz, 6H), 1.33–1.46 (m, 8H), 1.74–1.84 (m, 4H), 2.03 (s, 12H), 3.93 (t, $J=6.6$ Hz, 4H), 6.87 and 6.93 (AA'BB', $J=9.1$ Hz, 8H). Elemental analysis: calculated for $C_{32}H_{42}O_6$, C 73.53, H 8.10; found, C 73.56, H 8.12%.

Bis(4-hexyloxyphenyl) bicyclo[2.2.2]octane-1,4-dicarboxylate (1C[6]).

From pentane, 1H NMR: δ 0.91 (t, $J=6.8$ Hz, 6H), 1.31–1.38 (m, 8H), 1.40–1.49 (m, 4H), 1.77 (quint, $J=7.0$ Hz, 4H), 2.03 (s, 12H), 3.93 (t, $J=6.6$ Hz, 4H), 6.87 and 6.93 (AA'BB', $J=9.2$ Hz, 8H). Elemental analysis: calculated for $C_{34}H_{46}O_6$, C 74.15, H 8.42; found, C 74.23, H 8.45%.

Bis(4-heptyloxyphenyl) bicyclo[2.2.2]octane-1,4-dicarboxylate (1C[7]).

From pentane, 1H NMR: δ 0.89 (t, $J=7.0$ Hz, 6H), 1.25–1.49 (m, 16H), 1.77 (quint, $J=7.2$ Hz, 4H), 2.03 (s, 12H), 3.93 (t, $J=6.6$ Hz, 4H), 6.87 and 6.93 (AA'BB', $J=9.2$ Hz, 8H). Elemental analysis: calculated for $C_{36}H_{50}O_6$, C 74.71, H 8.71; found, C 74.74, H 8.68%.

Bis(4-octyloxyphenyl) bicyclo[2.2.2]octane-1,4-dicarboxylate (1C[8]).

From pentane, 1H NMR: δ 0.89 (t, $J=6.7$ Hz, 6H), 1.25–1.49 (m, 20H), 1.77 (quint, $J=7.2$ Hz, 4H), 2.03 (s, 12H), 3.93 (t, $J=6.6$ Hz, 4H), 6.87 and 6.93 (AA'BB', $J=9.2$ Hz, 8H). Elemental analysis: calculated for $C_{38}H_{54}O_6$, C 75.21, H 8.97; found, C 75.25, H 8.90%.

Bis(4-nonyloxyphenyl) bicyclo[2.2.2]octane-1,4-dicarboxylate (1C[9]).

From hexane, 1H NMR: δ 0.88 (t, $J=6.3$ Hz, 6H), 1.25–1.40 (m, 20H), 1.41–1.50 (m, 4H), 1.77 (quint, $J=7.3$ Hz, 4H), 2.03 (s, 12H), 3.93 (t, $J=6.5$ Hz, 4H), 6.86 (d, $J=9.0$ Hz, 4H), 6.94 (d, $J=9.1$ Hz, 4H). Elemental analysis: calculated for $C_{40}H_{58}O_6$, C 75.67, H 9.21; found, C 75.57, H 9.18%.

Bis(4-decyloxyphenyl) bicyclo[2.2.2]octane-1,4-dicarboxylate (1C[10]).

From hexane, 1H NMR: δ 0.88 (t, $J=6.0$ Hz, 6H), 1.25–1.37 (m, 24H), 1.38–1.49 (m, 4H), 1.76 (quint, $J=7.2$ Hz, 4H), 2.03 (s, 12H), 3.93 (t, $J=6.3$ Hz, 4H), 6.86 (d, $J=9.0$ Hz, 4H), 6.94 (d, $J=9.0$ Hz, 4H). Elemental analysis: calculated for $C_{42}H_{62}O_6$, C 76.09, H 9.43; found, C 76.22, H 9.51%.

Bis(4-dodecyloxyphenyl) bicyclo[2.2.2]octane-1,4-dicarboxylate (1C[12]).

From hexane and then MeCN, 1H NMR: δ 0.88 (t, $J=6.7$ Hz, 6H), 1.25–1.37 (m, 32H), 1.38–1.49 (m, 4H), 1.76 (quint, $J=7.3$ Hz, 4H), 2.03 (s, 12H), 3.93 (t, $J=6.6$ Hz, 4H), 6.86 (d, $J=9.1$ Hz, 4H), 6.94 (d,

$J=9.1$ Hz, 4H). Elemental analysis: calculated for $C_{46}H_{70}O_6$, C 76.84, H 9.81; found, C 77.07, H 9.82%.

1,4-Bis(4-pentyloxybenzoiloxy)bicyclo[2.2.2]octane (2C[5]).

Prepared according to a general procedure using 4-pentyloxybenzoyl chloride and bicyclo[2.2.2]octane-1,4-diol (23) and recrystallised from hexane. 1H NMR: δ 0.93 (t, $J=7.1$ Hz, 6H), 1.35–1.47 (m, 8H), 1.80 (quint, $J=7.0$ Hz, 4H), 2.33 (s, 12H), 3.99 (t, $J=6.6$ Hz, 4H), 6.87 (d, $J=8.9$ Hz, 4H), 7.90 (d, $J=8.9$ Hz, 4H). Elemental analysis: calculated for $C_{32}H_{42}O_6$, C 73.53, H 8.10; found, C 73.50, H 8.09%.

4-Nonyloxyphenol (66) (3[9]).

The phenol was prepared following a literature procedure for the decyloxy analogue (24) and recrystallised from isooctane: m.p. 70–71°C (lit. (66) m.p. 68.5°C). 1H NMR (300 MHz): δ 0.88 (t, $J=6.9$ Hz, 3H), 1.24–1.49 (m, 12H), 1.75 (quint, $J=7.4$ Hz, 2H), 3.89 (t, $J=6.6$ Hz, 2H), 4.4 (brs, 1H), 6.74 and 6.79 (AA'BB', $J=9.1$ Hz, 4H).

General procedure for 4-alkoxyphenol 3[n] $n \geq 12$.

To a suspension of NaH (440 mg, 11 mmol) in 20 ml of dry DMF was added hydroquinone (1.1 g, 10 mmol), and the mixture was stirred for 10 min at room temperature. An appropriate alkyl halide (11 mmol) was added, and the mixture was stirred at room temperature. The mixture was poured into 2N HCl aqueous solution, and extracted with CH_2Cl_2 , washed with brine, dried over $MgSO_4$ and evaporated. The crude mixture was purified by silica gel column chromatography with 1:10 AcOEt:*n*-hexane to give the corresponding 4-alkoxyphenol.

4-Dodecyloxyphenol (67) (3[12]).

Yield 38%; colourless leaflets ($CH_2Cl_2/MeOH$): m.p. 78–79°C (lit. (68) m.p. 79–80°C; lit. (67) m.p. 80–82°C). 1H NMR (270 MHz): δ 0.88 (t, $J=6.8$ Hz, 3H), 1.20–1.50 (brm, 18H), 1.75 (quint, $J=6.8$ Hz, 2H), 3.89 (t, $J=6.6$ Hz, 2H), 4.49 (s, 1H), 6.74 (d, $J=8.9$ Hz, 2H), 6.79 (d, $J=9.2$ Hz, 2H). MS (EI): m/z 278 (M^+), 110 (100 %). Elemental analysis: calculated for $C_{18}H_{30}O_2$, C 77.65, H 10.86; found, C 77.56, H 11.06%.

4-Tetradecyloxyphenol (67) (3[14]).

Yield 31%; colourless leaflets ($CH_2Cl_2/MeOH$): m.p. 76–78°C (lit. (68) m.p. 84–85°C; lit. (67) m.p. 85–86°C). 1H NMR (270 MHz, $CDCl_3$): δ 0.88 (t,

$J=6.9$ Hz, 3H), 1.20–1.50 (brm, 22H), 1.75 (quint, $J=6.9$ Hz, 2H), 3.89 (t, $J=6.8$ Hz, 2H), 6.74 (d, $J=9.2$ Hz, 2H), 6.78 (d, $J=9.2$ Hz, 2H). MS (EI): m/z 306 (M^+), 110 (100 %).

4-Hexadecyloxyphenol (67) (3[16]).

Yield 41%; colourless prisms ($CH_2Cl_2/MeOH$): m.p. 86–87°C (lit. (68) m.p. 88–89°C; lit. (67) m.p. 90–92°C). 1H NMR (600 MHz): δ 0.88 (t, $J=6.9$ Hz, 3H), 1.20–1.40 (brm, 24H), 1.43 (quint, $J=7.3$ Hz, 2H), 1.73 (quint, $J=7.3$ Hz, 2H), 3.89 (t, $J=6.6$ Hz, 2H), 4.39 (s, 1H), 6.75 (d, $J=9.2$ Hz, 2H), 6.78 (d, $J=9.2$ Hz, 2H). MS (EI): m/z 334 (M^+), 110 (100 %). Elemental analysis: calculated for $C_{22}H_{38}O_2$, C 78.99, H 11.45; found, C 78.99, H 11.68%.

4-Octadecyloxyphenol (67) (3[18]).

Yield 28%; brown prisms ($CH_2Cl_2/MeOH$): m.p. 91–92°C (lit. (67) m.p. 89–92°C). 1H NMR (270 MHz): δ 0.88 (t, $J=6.9$ Hz, 3H), 1.20–1.50 (brm, 30H), 1.74 (quint, $J=6.8$ Hz, 2H), 3.88 (t, $J=6.6$ Hz, 2H), 4.39 (s, 1H), 6.74 (d, $J=9.1$ Hz, 2H), 6.78 (d, $J=9.1$ Hz, 2H). MS (EI): m/z 362 (M^+), 110 (100 %). Elemental analysis: calculated for $C_{24}H_{42}O_2$, C 79.50, H 11.68; found, C 79.22, H 11.93%.

4-Eicosyloxyphenol (3[20]).

Yield 44%; colourless cotton-like ($CH_2Cl_2/MeOH$): m.p. 93–94°C. 1H NMR (600 MHz): δ 0.88 (t, $J=6.9$ Hz, 3H), 1.20–1.40 (brm, 32H), 1.43 (quint, $J=7.0$ Hz, 2H), 1.75 (quint, $J=6.9$ Hz, 2H), 3.89 (t, $J=6.6$ Hz, 2H), 4.41 (s, 1H), 6.75 (d, $J=9.5$ Hz, 2H), 6.78 (d, $J=9.2$ Hz, 2H). MS (EI): m/z 390 (M^+), 110 (100 %). Elemental analysis: calculated for $C_{26}H_{46}O_2$, C 79.94, H 11.87; found, C 79.73, H 11.78%.

4-Docosyloxyphenol (3[22]).

Yield 31%; pale pink cotton-like ($CH_2Cl_2/MeOH$): m.p. 98–100°C. 1H NMR (400 MHz): δ 0.88 (t, $J=7.1$ Hz, 3H), 1.20–1.40 (brm, 32H), 1.43 (quint, $J=6.6$, 2H), 1.75 (quint, $J=6.8$ Hz, 2H), 3.89 (t, $J=6.6$ Hz, 2H), 4.45 (s, 1H), 6.75 (d, $J=9.3$ Hz, 2H), 6.78 (d, $J=9.3$ Hz, 2H). MS (EI): m/z 418 (M^+), 110 (100 %).

Data collection and structure determination and refinement

A colourless crystal (approximate dimensions $0.40 \times 0.35 \times 0.30$ mm³ for **1A[3]**, $0.31 \times 0.30 \times 0.24$ mm³ for **1B[4]**, or $0.40 \times 0.20 \times 0.06$ mm³ for **1C[4]**) was placed onto the tip of a 0.1 mm diameter glass capillary and mounted on a Siemens SMART CCD

area detector diffractometer for a data collection at 173(2) K or 100(2) K (**1A[3]**). A preliminary set of cell constants was calculated from reflections harvested from three sets of 20 frames. These initial sets of frames were oriented such that orthogonal wedges of reciprocal space were surveyed. This produced initial orientation matrices determined from 105 reflections for **1A[3]**, 117 for **1B[4]**, and 35 for **1C[4]**. The data collection was carried out using Mo Ka radiation (graphite monochromator) with a frame time of 20 s. (**1A[3]** and **1B[4]**) or 60 sec. (**1C[4]**) and a detector distance of 4.9 cm. A randomly oriented region of reciprocal space was surveyed to the extent of one sphere and to a resolution of 0.84 Å. Four major sections of frames were collected with 0.30° steps in ω at four different ϕ settings and a detector position of -28° in 2θ . The intensity data were corrected for absorption and decay (SADABS) (69). Final cell constants were calculated from 1566 (**1A[3]**), 6115 (**1B[4]**), or 2029 (**1C[4]**) strong reflections from the actual data collection after integration (SAINT) (70). Additional crystal and refinement information are given in the footnote (45).

The structure was solved and refined using Bruker SHELXTL (71). The space groups *Pbca* (**1A[3]**), *P2₁/c* (**1B[4]**) and *P* (**1C[4]**) were determined based on systematic absences and intensity statistics. A direct-methods solution was calculated which provided most non-hydrogen atoms from the E-map. Several full-matrix least squares/difference Fourier cycles were performed which located the remaining non-hydrogen atoms. All non-hydrogen atoms were refined with anisotropic displacement parameters. All hydrogen atoms were placed in ideal positions and refined as riding atoms with relative isotropic displacement parameters. The final full matrix least squares refinement converged to $R1=0.0485$ and $wR2=0.1298$ for **1A[3]**, $R1=0.1236$ and $wR2=0.1354$ for **1B[4]**, or $R1=0.0436$ and $wR2=0.1333$ for **1C[4]**, (F^2 , all data).

In **1B[4]** the disordered alkyl chain in molecule **B** was split into separate parts and refined to 0.52:0.48 ratio of occupancy. The non-disordered end-alkyl chains were used as paradigm fragments coupled with the SHELXTL SAME restraint; 105 restraints were employed. The crystal of **1B[4]** diffracted poorly and data was recollected. The residuals did not change much despite doubling the exposure time from 10 to 20 seconds. The higher than expected residuals could be due to the disorder.

Supplementary materials

Crystallographic data for structural analysis of **1A[3]**, **1B[4]** and **1C[4]** has been deposited at the Cambridge

Crystallographic Data Centre, CCDC, No. 695355, 695357 and 695356, respectively. Copies of this information can be obtained from the Director, CCDC, 12 Union Road, Cambridge CB2 1EZ, UK (fax: +44 1233 336033, Email: deposit@ccdc.cam.ac.uk or www.ccdc.cam.ac.uk).

Acknowledgements

This project was supported in part by the NSF grants (DMR-0111657 and DMR-0606317) and by Grant-in-Aid for Scientific Research (B) No.13470468, the Ministry of Education, Culture, Sports, Science and Technology, Japan. We thank to Dr. Jadwiga Laska and Dr. Andrew G. Douglass for their help with obtaining the X-ray quality crystal of **1B[4]**. We also thank Prof. Roman Dabrowski for the gift of 4-decyloxyphenol (**3[10]**).

References

- (1) Vill V., *LiqCryst* 4.6, ed. Harris, N.; Sajus, H.; Peters, G. 2002, LCI Publisher GmbH, Hamburg, Germany, database and references therein.
- (2) Deutscher H.J.; Frach R.; Tschierske C.; Zschke H. In *Selected Topics in Liquid Crystal Research*; Koswig H.-D. (Eds), Akademie-Verlag: Berlin, 1990, p1–18 and references therein.
- (3) Vill V.; Thiem J. *Z. Naturforsch.* **1990**, *45A*, 1345–1348.
- (4) Kleinpeter E.; Köhler H.; Lunow A.; Tschierske C.; Zschke H. *Tetrahedron* **1988**, *44*, 1609–1612.
- (5) Kaszynski P.; Pakhomov S.; Tesh K.F.; Young V.G., Jr. *Inorg. Chem.* **2001**, *40*, 6622–6631.
- (6) Piecek W.; Kaufman J.M.; Kaszynski P. *Liq. Cryst.* **2003**, *30*, 39–48.
- (7) Douglass A.G.; Both B.; Kaszynski P. *J. Mater. Chem.* **1999**, *9*, 683–686.
- (8) Kaszynski P.; Douglass A.G. *J. Organomet. Chem.* **1999**, *581*, 28–38.
- (9) (a) Douglass A.G.; Czuprynski K.; Mierzwa M.; Kaszynski P. *Chem. Mater.* **1998**, *10*, 2399–2402; (b) Douglass, A.G.; Czuprynski, K.; Mierzwa, M.; Kaszynski, P. *J. Mater. Chem.* **1998**, *8*, 2391–2398; (c) Czuprynski, K.; Kaszynski, P. *Liq. Cryst.* **1999**, *26*, 775–778; (d) Czuprynski, K.; Douglass, A.G.; Kaszynski, P.; Drzewinski, W. *Liq. Cryst.* **1999**, *26*, 261–269; (e) Ohta, K.; Januszko, A.; Kaszynski, P.; Nagamine, T.; Sasnouski, G.; Endo, Y. *Liq. Cryst.* **2004**, *31*, 671–682; (f) Januszko, A.; Kaszynski, P.; Wand, M.D.; More, K.M.; Pakhomov, S.; O'Neill, M. *J. Mater. Chem.* **2004**, *14*, 1544–1553; (g) Ringstrand, B.; Vroman, J.; Jensen, D.; Januszko, A.; Kaszynski, P.; Dziaduszek, J.; Drzewinski, W. *Liq. Cryst.* **2005**, *32*, 1061–1070; (h) Januszko, A.; Glab, K.L.; Kaszynski, P.; Patel, K.; Lewis, R.A.; Mehl, G.H.; Wand, M.D. *J. Mater. Chem.* **2006**, *16*, 3183–3192; (i) Januszko, A.; Glab, K.L.; Kaszynski, P. *Liq. Cryst.* **2008**, *35*, 549–553; (j) Januszko, A.; Kaszynski, P. *Liq. Cryst.* **2008**, *35*, 705–710; (k) Jasinski, M.; Jankowiak, A.; Januszko, A.; Bremer, M.; Pauluth, D.; Kaszynski, P. *Liq. Cryst.* **2008**, *35*, 343–350; (l) Nagamine, T.; Januszko, A.; Ohta, K.; Kaszynski, P.; Endo, Y. *Liq. Cryst.* **2008**, *35*, 865–884.

- (10) Nagamine T.; Januszko A.; Kaszynski P.; Ohta K.; Endo Y. *J. Mater. Chem.* **2006**, *16*, 3836–3843.
- (11) Nagamine T.; Januszko A.; Ohta K.; Kaszynski P.; Endo Y. *Liq. Cryst.* **2005**, *32*, 985–995.
- (12) Januszko A.; Kaszynski P.; Drzewinski W. *J. Mater. Chem.* **2006**, *16*, 452–461.
- (13) Kaszynski P.; Kulikiewicz K.K.; Januszko A.; Douglass A.G.; Tilford R.W.; Pakhomov S.; Patel M.K.; Radziszewski G.J.; Young V.G., Jr. .to be submitted for publication.
- (14) Neubert M.E.; Ferrato J.P.; Carpenter R.E. *Mol. Cryst. Liq. Cryst.* **1979**, *53*, 229–252.
- (15) Cox R.J. In *The Physics and Chemistry of Liquid Crystal Devices*; Sprokel G.J. (Ed.), Plenum Press: New York, 1980. pp. 295–303.
- (16) Kelker H.; Scheurle B. *J. Phys., Paris* **1969**, *30-C4*, 104–108.
- (17) Dewar M.J.S.; Goldberg R.S. *J. Org. Chem.* **1970**, *35*, 2711–2715.
- (18) Cai R.; Samulski E.T. *Liq. Cryst.* **1991**, *9*, 617–634.
- (19) (a) Kahl S.B.; Kasar R.A. *J. Am. Chem. Soc.* **1996**, *118*, 1223–1224; (b) Zakharkin, L.I.; Kalinin, V.N.; Podvisotskaya, L.S. *Bull. Acad. Sci. USSR, Div. Chem. Sci.* **1968**, 2532.
- (20) Garrett P.M.; Smart J.C.; Hawthorne M.F. *J. Am. Chem. Soc.* **1969**, *91*, 4707–4709.
- (21) Kauer J.C.; Benson R.E.; Parshall G.W. *J. Org. Chem.* **1965**, *30*, 1431–1436.
- (22) von Gersdorff J.; Kirste B.; Niethammer D.; Harrer W.; Kurreck H. *Mang. Res. Chem.* **1988**, *26*, 416–424.
- (23) Dewar M.J.S.; Goldberg R.S. *J. Am. Chem. Soc.* **1970**, *92*, 1582–1586.
- (24) Saes I.M.; Mehl G.H.; Sinn E.; Styring P. *J. Organomet. Chem.* **1998**, *551*, 299–311.
- (25) Connolly S.; Bennion C.; Botterell S.; Croshaw P.J.; Hallam C.; Hardy K.; Hartopp P.; Jackson C.G.; King S.J.; Lawrence L., et al. *J. Med. Chem.* **2002**, *45*, 1348–1362.
- (26) (a) Demus D.; Richter L. *Textures of Liquid Crystals* **1980** 2nd ed.; VEB, (b) Gray, G.W.; Goodby, J.W.G. *Smectic Liquid Crystals-Textures and Structures*; Leonard Hill: Philadelphia, 1984; (c) Dierking, I. *Textures of Liquid Crystals*; Wiley-VCH: Weinheim, 2003.
- (27) Diester **1E[10]** has a 3 K wide nematic phase (34) and diester **1E[12]** is reported by V. Vill in *LiqCryst* database (*I*; #34715) to possess only a SmC phase. Therefore, it is possible that the unknown diester **1E[11]** has no nematic phase.
- (28) Gray G.W.; Langley N.A.; Toyne K.J. *Mol. Cryst. Liq. Cryst.* **1981**, *64*, 239–245.
- (29) Geyvandov R.C.; compound #34715 in *LiqCryst* database (*I*); ref #5294.
- (30) Dewar M.J.S.; Griffin A.C. *J. Am. Chem. Soc.* **1975**, *97*, 6662–6666.
- (31) Dewar M.J.S.; Griffin A.C. *J. Chem. Soc., Perkin Trans 2* **1976**, 710–713.
- (32) Takenaka S.; Sakurai Y.; Takeda H.; Ikemoto T.; Miyake H.; Kusabayashi S.; Takagi T. *Mol. Cryst. Liq. Cryst.* **1990**, *178*, 103–115.
- (33) Andrews J.T.S.; Bacon W.E. *J. Chem. Thermodynamics* **1974**, *6*, 515–523.
- (34) Neubert M.E.; Wildman P.J.; Zawaski M.J.; Hanlon C.A.; Benyo T.L.; De Vries A. *Mol. Cryst. Liq. Cryst.* **1987**, *145*, 111–157.
- (35) Thiem J.; Vill V.; Fischer F. *Mol. Cryst. Liq. Cryst.* **1989**, *170*, 43–51.
- (36) (a) Becke A.D. *J. Chem. Phys.* **1993**, *98*, 5648–5652; (b) Lee, C.; Yang, W.; Parr, R.G. *Phys. Rev. B* **1988**, *37*, 785–789; (c) Møller, C.; Plesset, M.S. *Phys. Rev.* **1934**, *46*, 618–622; (d) Head-Gordon, M.; Pople, J.A.; Frisch, M.J. *Chem. Phys. Lett.* **1988**, *153*, 503–506.
- (37) Frisch M.J.; Trucks G.W.; Schlegel H.B.; Scuseria G.E.; Robb M.A.; Cheeseman J.R.; Zakrzewski V.G.; Montgomery J.A., Jr.; Stratmann R.E.; Burant J.C., et al. *Gaussian 98* **1998** revision A.9, Gaussian, Inc: Pittsburgh, PA, 1998.
- (38) Sridhar M.A.; Lokanath N.K.; Krishnegowda D.; Revanasiddaiah D.; Shashidhara P.J. *Mol. Cryst. Liq. Cryst.* **1997**, *299*, 509–515.
- (39) Kaszynski P.; Pakhomov S.; Young V.G., Jr. *Coll. Czech. Chem. Commun.* **2002**, *67*, 1061–1083.
- (40) van Koningsveld H.; Jansen J.C. *Acta Crystallogr.* **1984**, *B40*, 420–424.
- (41) Baumeister U.; Brandt W.; Hartung H.; Wedler W.; Deutscher H.-J.; Frach R.; Jaskolski M. *Mol. Cryst. Liq. Cryst.* **1985**, *130*, 321–336.
- (42) von Luger P.; Plieth K.; Ruban G. *Acta Crystallogr.* **1972**, *B28*, 706–710.
- (43) Allouchi H.; Cotrait M.; Guillon D.; Heinrich B.; Hguyen H.T. *Chem. Mater.* **1995**, *7*, 2252–2258.
- (44) Badawi H.M. *J. Mol. Struct. (THEOCHEM)* **1996**, *369*, 75–83.
- (45) Crystal data for **1A[3]**: C₂₂H₃₂B₁₀O₆ orthorhombic, *Pbca*, *a*=9.8636(17) Å, *b*=8.8162(15) Å, *c*=30.986(5) Å, *V*=2694.6(8) Å³, *Z*=4, *T*=173(2) K, λ =0.71073 Å, *R*(*F*²)=0.0485 or *R*_w(*F*²)=0.1098 (for 1698 reflections with *I*>2σ(*I*)). Crystal data for **1B[4]**: C₂₄H₃₄B₈O₆ monoclinic, *P2₁/c*, *a*=10.3175(2) Å, *b*=31.2319(7) Å, *c*=26.1744(5) Å, β =96.908(1)°, *V*=8373.1(3) Å³, *Z*=12, *T*=173(2) K, λ =0.71073 Å, *R*(*F*²)=0.0683 or *R*_w(*F*²)=0.1174 (for 9067 reflections with *I*>2σ(*I*)). Crystal data for **1C[4]**: C₃₀H₃₈O₆ triclinic, *P*, *a*=6.2417(9) Å, *b*=11.2531(16) Å, *c*=19.516(3) Å, α =74.598(2)°, β =89.980(2)°, γ =83.931(2)°, *V*=1313.6(3) Å³, *Z*=2, *T*=100(2) K, λ =0.71073 Å, *R*(*F*²)=0.0436 or *R*_w(*F*²)=0.1110 (for 3311 reflections with *I*>2σ(*I*)).
- (46) Pakhomov S.; Kaszynski P.; Young V.G., Jr. *Inorg. Chem.* **2000**, *39*, 2243–2245.
- (47) Haase W.; Athanassopoulou M.A. In *Structure and Bonding*; Mingos D.M.P. (Eds), Springer: Berlin, 1999, Vol. 94, pp 139–197, and references therein.
- (48) (a) Gray G.W. *Molecular Structure and the Properties of Liquid Crystals*; Academic Press: New York, 1962, pp 197–238; (b) Gray, G.W. in *Liquid Crystals and Plastic Crystals*, Vol. 1; Gray, G.W., Winsor, P.A., Eds; Wiley & Sons: New York, 1974; pp 103–152; (c) Gray, G.W. In *Advances in Liquid Crystals*, Vol. 2; Brown, G.H., Ed.; Academic Press: New York, 1976; pp 1–72, and references therein.
- (49) Demus D.; Hauser A. In *Selected Topics In Liquid Crystal Research*; Koswig H.-D. (Ed.), Akademie-Verlag: Berlin, 1990. pp. 19–44.
- (50) de Jeu W.H.; van der Veen J.; Goossens W.J.A. *Solid St. Commun* **1973**, *12*, 405–407; see also: Kaplan, J.I. *J. Chem. Phys.* **1972**, *57*, 3015.
- (51) For instance, (a) Maier, W.; Saupe, A. *Z. Naturforsch* **1959**, *14a*, 882–889; (b) Maier, W.; Saupe, A. *Z. Naturforsch.* **1960**, *15a*, 287–292; (c) Pink, D.A. *J. Chem. Phys.* **1975**, *63*, 2533–2539; (d) Marcelja, S. J.

- Chem. Phys.* **1974**, *60*, 3599–3604. See also: Demus, D. *Z. Chem.* **1975**, *15*, 1–14, and references therein.
- (52) Gray G.W. In *Polymer Liquid Crystals*; Ciferri A., Krigbaum W.R., Meyer R.B. (Eds), Academic Press: New York, 1982. pp. 8–9.
- (53) In the general case, the clearing temperature of the diaxial conformer $T_{MI}(aa)$ can be expressed as a fraction a of the clearing temperature of the diequatorial conformer, which leads to the expanded form of Equation (5): $T_{MI}(aa) = T_{MI}(D) \cdot K + 1 / (a \cdot K + 1)$. For simplicity, parameter a is assumed to be 0. However, the value of a defines the average difference $\Delta T_{MI} = T_{MI}(ee) - T_{MI}(E)$ and the steric energy; for increasing values of a the ΔT_{MI} increases and ΔG decreases. Conversely, as the parameter a decreases below 0, the ΔT_{MI} also decreases and ΔG increases.
- (54) For the purpose of this discussion ΔS is assumed to be 0, which makes ΔG temperature independent. The reported ΔS value for a single COOR group in *t*-BuOH is $0.4 \pm 0.1 \text{ cal mol}^{-1} \text{ K}^{-1}$ (57) and in ether/toluene- d_8 $-0.6 \pm 0.8 \text{ cal mol}^{-1} \text{ K}^{-1}$ (Booth, H.; Dixon, J.M.; Khedhair, K.A. *Tetrahedron* **1992**, *48*, 6161–6174). However, the exact value of entropy change is not essential for the purpose of this discussion.
- (55) Deutscher H.-J.; Laaser B.; Dölling W.; Schubert H. *J. Prakt. Chem.* **1978**, *320*, 191–205.
- (56) (a) Neubert M.E.; Carlino L.T.; Fishel D.L.; D'sidocky R.M. *Mol. Cryst. Liq. Cryst.* **1980**, *59*, 253–272; (b) van Meter, J.P.; Klanderman, B.H. *Mol. Cryst. Liq. Cryst.* **1973**, *22*, 271–284.
- (57) Ouellette R.J.; Booth G.E. *J. Org. Chem.* **1966**, *31*, 587–588.
- (58) Jensen F.R.; Bushweller C.H. *Adv. Alicyclic Chem.* **1971**, *3*, 185–190, and references therein. See also: Zefirov, N.S. *Tetrahedron Lett.* **1975**, *13*, 1087–1090; Abraham, R.J.; Rossetti, Z.L. *J. Chem. Soc., Perkin Trans II* **1973**, 582–587; Kleinpeter, E.; Köhler, H.; Tschierske, C.; Zschke, H. *J. Prakt. Chem.* **1988**, *330*, 484–486; Kleinpeter, E.; Köhler, H.; Krieg, R.; Deutscher, H.-J. *J. Prakt. Chem.* **1989**, *331*, 171–174.
- (59) Borsdorf R.; Arnold M.; Kleinpeter E. *Z. Chem.* **1977**, *17*, 378–379.
- (60) Zefirov N.S.; Samoshin S.S.; Nikulin A.V.; Zyk N.V. *J. Org. Chem. USSR* **1978**, *14*, 2407–2408.
- (61) Jensen F.R.; Bushweller C.H.; Beck B.H. *J. Am. Chem. Soc.* **1969**, *91*, 344–351.
- (62) For example, Centore, R.; Tuzi, A. *Acta Crystallogr.* **1998**, *C54*, 107–109; Tamura, K.; Hori, K. *Bull. Chem. Soc. Japan* **2000**, *73*, 843–850.
- (63) Balinski A.; Januszko A.; Harvey J.E.; Kaszynski P.; Brady E.; Young V.G., Jr. to be submitted for publication.
- (64) Ermer O.; Dunitz J.D. *Helv. Chim. Acta* **1969**, *52*, 1861–1886.
- (65) In dibenzoate **2D[16]** the nematic phase is completely replaced with a SmC phase (35).
- (66) Klarmann E.; Gatyas L.W.; Shternov V.A. *J. Am. Chem. Soc.* **1932**, *54*, 298–305.
- (67) Neubert M.E.; Laskos S.J., Jr.; Maurer L.J.; Carlino L.T.; Ferrato J.P. *Mol. Cryst. Liq. Cryst.* **1978**, *44*, 197–210.
- (68) Byron D.J.; Lacey D.; Wilson R.C. *Mol. Cryst. Liq. Cryst.* **1979**, *51*, 265–272.
- (69) An empirical correction for absorption anisotropy, Blessing, R.H. *Acta Crystallogr.* **1995**, *A51*, 33–38.
- (70) *SAINTE V6.2*; Bruker Analytical X-Ray Systems: Madison, WI, 2001.
- (71) *SHELXTL V6.10*; Bruker Analytical X-Ray Systems: Madison, WI, 2000.